Dynamics of local protein synthesis in cortical neuronal dendrites and their regulation: Examining the effects of 3'UTRs in mRNA localisation and translation

Author:
Leah Broger
Radboud University, Nijmegen, The Netherlands

Supervisor:
Dr. Erin Schuman, PhD
Max Planck Institute for Brain Research & Radboud University

Secondary Reader:
Dr. Anne-Sophie Hafner, PhD
Radboud University

A thesis submitted in partial fulfilment of the requirements for the degree

Research Master in Cognitive Neuroscience

Table of Contents

Table of Figures

Abstract

Neurons adjust the types and levels of proteins they produce in response to changes in synaptic transmission. It was initially believed that protein translation was confined to the somatic space. However, ample evidence has shown that these processes occur in localised, remote regions far from the central nucleus[1]. This ability to autonomously adapt the local proteome – which refers to all the proteins a cell produces – allows neurons to respond dynamically to changes in their environment[2]. The need for local and independent protein synthesis in distal dendrites is crucial for synaptic plasticity to occur[3,4], as it allows for quick responses to changes in neural activity. It also enables neurons to overcome the logistical challenges associated with rapidly transporting new proteins from the soma to distal sites[5].

Understanding how neurons regulate the production of different proteins is crucial to appreciate how the brain processes information and adapts to new situations. Gaining a deeper insight into the mechanisms that govern protein synthesis could have far-reaching implications for treating neurological disorders related to imbalances in protein synthesis, degradation, and disruptions in synaptic function. Examples of such diseases include Autism Spectrum Disorders, Fragile X Syndrome, and Alzheimer's disease[6,7]. It has been shown that the localisation motifs required for transporting mRNAs are found in the 3' untranslated region (UTR)[8–12]. Therefore, a valuable way to visualise local protein synthesis has been to design and implement fluorescent reporters containing 5' and 3' UTRs of candidate mRNAs[13,14].

Although there is an abundance of research on the translation of mRNAs and local synthesis of proteins at the synapse, the dynamic visualisation of local protein synthesis *in vivo* during learning and memory has yet to be realised. Currently, Dr. Donlin-Asp and Teresa Spanò in the Schuman lab are addressing this question by using fluorescent reporters with UTRs from *Beta Actin* and *Psd95* to visually analyse local protein synthesis dynamics and regulation *in vivo*. To ensure that these reporters are robust tools to measure local translation, this thesis project aims to visualise the spatial distribution and expression of these mRNA reporters compared to their endogenous correlates.

We demonstrate that our candidate reporters are enriched in dendrites compared to a control lacking a 3' UTR sequence by analysing the puncta count of mRNAs after fluorescent *in situ* hybridisation. Moreover, we determine that our reporter constructs' distribution closely parallels that of endogenous *Beta Actin* and *Psd95* mRNAs in culture. Lastly, we show the successful integration of puromycin into the nascent peptide chain as a proof-of-concept for an eventual puromycin proximity ligation assay on our reporters[15]. This would enable us to see where protein synthesis occurs. Future directions for validating mRNA localisation *ex vivo* involve applying the approaches outlined in this thesis to tissue slices.

Acknowledgements

This thesis could not have been completed without external support. I would like to thank Prof. Dr. Erin M. Schuman for the opportunity to work in her lab alongside many incredibly talented and ambitious scientists and for introducing me to an exciting and experimentally challenging project, and Dr. Anne-Sophie Hafner for her continued support and organizational cooperation. I would also like to thank Dr. Paul Donlin-Asp and Teresa Spanò for allowing me to participate in their research. From their day-to-day supervision to assisting with experiments and providing constructive criticism for my lab meeting and written work, their input was instrumental in helping me piece my experiments into a cohesive story.

In addition, I would like to thank Ina Bartnik and Belquis Nassim for their guidance and instruction in various lab techniques and for preparing our neuronal cell cultures. Mainly I would like to thank Belquis Nassim for her help troubleshooting the *in-situ* hybridization protocol, Anita Kulak, for her managerial skills, kindness, and constant positive energy, and Mara Müller for letting me use her cells on multiple occasions and providing me with her ImageJ macro script as a tentative analysis pipeline. Melissa Hahn and Kim Verdaasdonk, for being great colleagues, supportive friends, and ambitious aspiring scientists. Lastly, I would like to thank the entire Schuman Lab for the stimulating lunch discussions, valuable feedback, and encouraging atmosphere.

1. Introduction

1.1 Synaptic Plasticity in Learning and Memory

Over the last decades, significant efforts have been made to understand the brain's remarkable capability to integrate information and store memories. It is estimated that the brain is home to roughly 86 billion neurons[16], which possess discrete morphological features that allow information to be processed and transmitted on the order of milliseconds[17]. Neurons can alter the strength and frequency of transmission during experience-dependent activity in a malleable and reversible fashion; this process is known as synaptic plasticity[18,19]. Plasticity is bidirectional, meaning the synapse can either be potentiated or depressed[18].

At the molecular level, synaptic plasticity is governed by many distinct and complex mechanisms that alter the proteomic landscape of individual synapses[18]. Roughly 2,500 protein species have been identified at the synapse[3,20]. Since individual protein species exist in multiple copies, the total number of molecules is significantly greater, on the order of millions[21]. These include scaffold proteins that initiate signalling cascades[22] such as CAMKII (5000 copies) and Psd95 (300 copies), neurotransmitter receptors (30–80 copies), and ion channels (200-400 copies), amongst others[23]. Proteins have a short lifespan – typically measured in days or weeks depending on the specific protein – and are constantly being synthesised and degraded in cells[24,25]. This rapid turnover of proteins is necessary for cellular homeostasis, which relies on the necessary protein supply. However, this process becomes even more critical in the context of synaptic plasticity, where proteins must be produced and degraded at the synapse promptly. To meet this need, cells have evolved a mechanism for local protein synthesis in dendrites.

The first studies to propose the necessity of protein synthesis for learning and memory used protein synthesis inhibitors. They detected that memory retention was effectively impaired when protein synthesis in the brain was chemically blocked[26]. Subsequent work substantiated that *de novo* protein synthesis shortly after learning was critical for memory consolidation[27]. A robust example of this was seen in knockout studies with mice lacking key protein synthesis molecules, which caused deficiencies in learning and phenotypic changes in plasticity[28–30]. These studies demonstrated the need for protein synthesis during learning and memory and the rapid proteomic changes that occur during synaptic plasticity.

This led to a renewed focus on understanding the mechanisms and regulation of protein synthesis in these remote regions of the neuron. It is generally true that many proteins are synthesised in the cell body – also known as the soma – and then transported to distal parts of the neuron such as dendrites and axons[31,32]. In active transport, proteins synthesised in the soma are transported to the dendrites via different transport mechanisms. One of the most widely accepted mechanisms is microtubule-dependent transport. In this process, proteins are transported along microtubules, which are long, cylindrical structures and one of the three classes of cytoskeletal systems that help form the structural "skeleton" of the cell[32]. Given that synaptic plasticity occurs on a very short time scale[18] – with changes happening in milliseconds to seconds – it is difficult to understand how the slow process of protein transport from the cell body to distal sites can keep up with the necessary demand in these areas. It is now believed that an alternative mechanism neurons exploit to overcome these limitations is the local synthesis of proteins in distal sites where these proteins are required[33]. This process is termed local translation and is actively regulated to ensure the appropriate protein levels are present at the synapse.

1.2 mRNA Localisation and Local Protein Synthesis

Speculation of protein synthesis in distal dendrites and axons surfaced as early as the 1960s, with studies revealing the incorporation of labelled amino acids into the nascent polypeptide chain in synaptosomal preparations[34,35]. Subsequently, Steward et al. (1982)[36] discovered multiple ribosomes associated with a single mRNA (polyribosomes) in distal dendritic spines. These polyribosomes also accumulated in spines during long-term potentiation (LTP) – a type of synaptic plasticity – which supported the idea that potentiated synapses actively produced protein[37,38]. These results, along with mRNA detection in dendrites and axons[8,39,40], spearheaded the hypothesis that neurons could produce protein locally, especially during plasticity. However, the functional role of this local protein synthesis was unknown.

In a ground-breaking study from Kang and Schuman in 1996[41], the first functional role for local protein synthesis in neurons was identified. Their research revealed that brain-derived neurotrophic factor (BDNF) – a growth factor resulting in a strongly potentiated plasticity state[4] – enhanced LTP and that this potentiation was protein synthesis-dependent. However, this dependency occurred rapidly, which did not seem consistent with the transport dynamics of proteins from the soma. This incited the idea that perhaps the proteins required for this

plasticity were being synthesised locally. They assessed this by isolating the cell bodies from the dendrites and axons (neuropil), where the recording electrode was placed in rat hippocampal slices. Notably, when BDNF was administered, the potentiation remained intact and was still protein synthesis-dependent, showing similar behaviour to sham-lesioned slices. These data conclusively demonstrated local protein synthesis in the neuropil to be required for the establishment and maintenance of BDNF potentiation. Based on these findings, a couple of years later, Huber et al. (2000)[42] used a similar approach for metabotropic glutamate receptor long-term depression (mGluR-LTD), successfully showing that mGluR-LTD – which is protein synthesis-dependent – was preserved in the neuropil of the stratum radiatum after excising the cell body layer of CA1. These experiments proved that local protein synthesis was necessary for multiple forms of synaptic plasticity.

To facilitate protein production at the site of action, it is essential that the mRNAs coding for these proteins are also readily transported near synapses. Recent research studies led by Dr. Erin Schuman and colleagues discovered thousands (~4500) of transcripts in the hippocampal neuropil[43]. The variety of mRNA species and the ability to synthesise proteins in various parts of the neuron suggests that local protein synthesis is a widely employed mechanism to adjust the number of proteins at the synapse, thus controlling the strength of synapses in a dynamic manner[44].

The processes involved in the transport and dynamics of mRNAs have been pivotal in understanding how mRNAs are recruited to synapses and translated to meet local cell demand. The literature suggests that a non-coding regulatory sequence found downstream of the coding sequence of mRNAs termed the 3' untranslated region (3' UTR) is significant in how and where these mRNAs are selectively transported, localised, and translated[11,45,46]. The 3'UTR region is known to hold most of the information for localisation due to its high affinity for RNA-binding proteins (RBPs) [11]. RBPs assemble on mRNAs during transcription and transport them from the cell body to distal dendrites in a translationally inactive state[47,48]. The release of mRNAs – which usually reside in RNA granules as they are transported – only occurs when protein synthesis is needed[49].

1.3 Visualising Local Protein Synthesis

Following Kang and Schuman's work[4,41], the necessity for local protein synthesis was further demonstrated in various lesion studies where axons were surgically isolated from their cell bodies[50–53]. However, while this technique showed the requirement for local protein synthesis, it did not provide a temporal account of local protein synthesis in a physiological context.

One method to visualise local protein synthesis is translating ribosome affinity purification (TRAP), which involves labelling a ribosomal protein with a fluorescent tag and then using immunoprecipitation to select mRNA populations bound to these ribosomes, thereby selecting for the mRNAs actively being translated in a specific cell type[54]. One critical study utilising this technique was Shigeoka et al. (2016)[55], which used an axon-TRAP-RiboTag method in mice to analyze ribosome-bound mRNAs in retinal ganglion cell axons in developing and adult retinas. The results showed that the mRNA translation profile changes over time and varies during different stages of axon wiring, including elongation, pruning, and synaptogenesis. Although TRAP is advantageous due to its ability to provide information on protein production in real-time, it is limited to actively translating mRNAs *ex vivo*, lacks spatial resolution, and can only capture a single, momentary reading.

Another way to identify newly synthesised proteins is by metabolic labelling methods that mark or tag these proteins. These techniques include incorporating non-canonical amino acids such as azidohomoalanine into proteins[56]. An application of this labelling was developed to detect nascent protein *in situ* using fluorescent labelling and click-chemistry, called fluorescence noncanonical amino acid tagging (FUNCAT)[57]. Puromycin is a drug often used as a metabolic label in visualization experiments. It is a synthetic antibiotic that mimics the action of the aminoacyl-tRNA and binds to the ribosome, causing premature termination of protein synthesis[58]. When added to cells, puromycin incorporates itself into newly synthesized proteins, which can then be detected using specific antibodies to track the translation of specific mRNAs in real-time. These methods allow *in situ* detection of newly synthesised proteins, which helps study protein synthesis in a specific cellular location. One limitation of the FUNCAT method is that it requires samples to be fixed, which means that the sample is chemically treated to preserve it for analysis. This can make it difficult to study dynamic processes, such as protein synthesis, that are occurring in live cells.

In addition, fluorescent reporters have been used to visually track mRNA translation in living dendrites at high temporal resolution. These reporters typically consist of an mRNA molecule containing a fluorescent protein sequence that can emit a signal when translated[59]. One of the first studies to implement fluorescent reporters was Aakalu et al. (2001)[13]. For their experiments, constructs were designed to contain the sequence encoding a green fluorescent protein (GFP) and the 5' and 3' UTR from *CamkIIa* mRNA[60,61], as these regions were shown to have sequences necessary for dendritic localisation. The reporter constructs were then transduced into cultured hippocampal cells and exposed to BDNF potentiation. They then conducted a time-lapsed experiment in hippocampal dendrites, using the GFP fluorescent signal as a proxy for protein synthesis. After BDNF administration, they observed a simultaneous increase in fluorescence signal in cell bodies and remote dendritic hotspots. The final confirmation of their findings was obtained by using optical techniques to separate the dendrites from the cell bodies and observing the presence of hotspots in the dendrites even after this separation.

A study on Aplysia neurites used a similar approach by implementing reporters of an Aplysia sensory neuron-specific peptide sensorin with photoconvertible fluorophores. The reporters were found to translate exclusively in stimulated synapses[62]. Translational reporters with fast-folding fluorescent proteins have also been implemented in fluorescence recovery after photobleaching (FRAP) studies. They have demonstrated dendritic protein synthesis in hippocampal neurons and retinal growth cones[63–65]. Notably, most of these studies have been *in vitro*, and it remains unclear if the same local translational dynamics appear *in vivo*. One exception to this has been the work of Wong et al. (2017)[66], which used FRAP to study protein synthesis in developing growth cones of Xenopus laevis. This study was the first to use FRAP to study protein synthesis *in vivo* in developing neurons. The results showed that newly synthesized proteins were rapidly incorporated into the growth cone, supporting the idea that local protein synthesis is important for growth cone function. By studying local protein synthesis *in vivo*, it is evident that we obtain a more complete understanding of how these processes occur in a living organism.

1.4 Project Background: Analysing Local Protein Synthesis *in vivo*

Previous transcriptomic studies by the Schuman lab have shown that mRNAs are localised to distal dendrites and axons *in vivo*[43]. However, studies have yet to dynamically track local translation in real-time in an intact brain, leaving a critical unresolved question: What is the functional role of local protein synthesis *in vivo*, and how are neurons using protein synthesis *in vivo* during learning and memory?

Current work by Dr. Paul Donlin-Asp and Teresa Spanò in the Schuman lab addresses this by using an *in vivo* system wherein local protein synthesis can be visualised. Their model focuses on the outmost part of the mouse cortex, layer I, as it is readily accessible and predominantly free from cell bodies compared to deeper cortical layer. In addition, layer I has been hypothesised to be a location necessary for learning[67].

To dynamically visualise local translation in layer I, a framework similar to that of Donlin-Asp et al.[14] is utilised, whereby translational reporters for two candidate mRNAs, *Beta Actin* and *Psd95,* are expressed. *Beta Actin* is one of the two non-muscle cytoskeletal actins – highly conserved proteins involved in cell motility – and is thought to play a role in the structural stability of dendritic spines[68], whereas *Psd95* is a pivotal postsynaptic scaffolding protein in excitatory neurons. Both proteins are abundant at postsynaptic dendritic spines and have mRNAs that localise to dendrites[69–74], making them strong candidates to study local translation. In addition, both proteins are implicated in synaptic plasticity [75–79].

To visualize protein synthesis in real-time, the reporters contain the coding sequence of a fast-folding fluorescent protein – Venus – whose mRNA is targeted to dendrites using the 3'UTR of the endogenous *Beta Actin* and *Psd95* mRNAs (Fig. 1A-B). These reporters are expressed in a Cre-dependent manner which ensures sparse (conditional) labelling in dendrites of a cell-type of interest (Fig. 1C). Comparing Venus fluorescence recovery after photobleaching and its dynamics to that of a negative control whose mRNA is not localised to dendrites (no UTR) allows us to infer how much of our construct is being translated locally. One of the caveats of using fluorescent proteins to study localised translation is their ability to diffuse freely within cells. Therefore, adding a myristoylation (myr) sequence anchors the protein to the membrane and limits its diffusion, providing stronger spatial information[80].

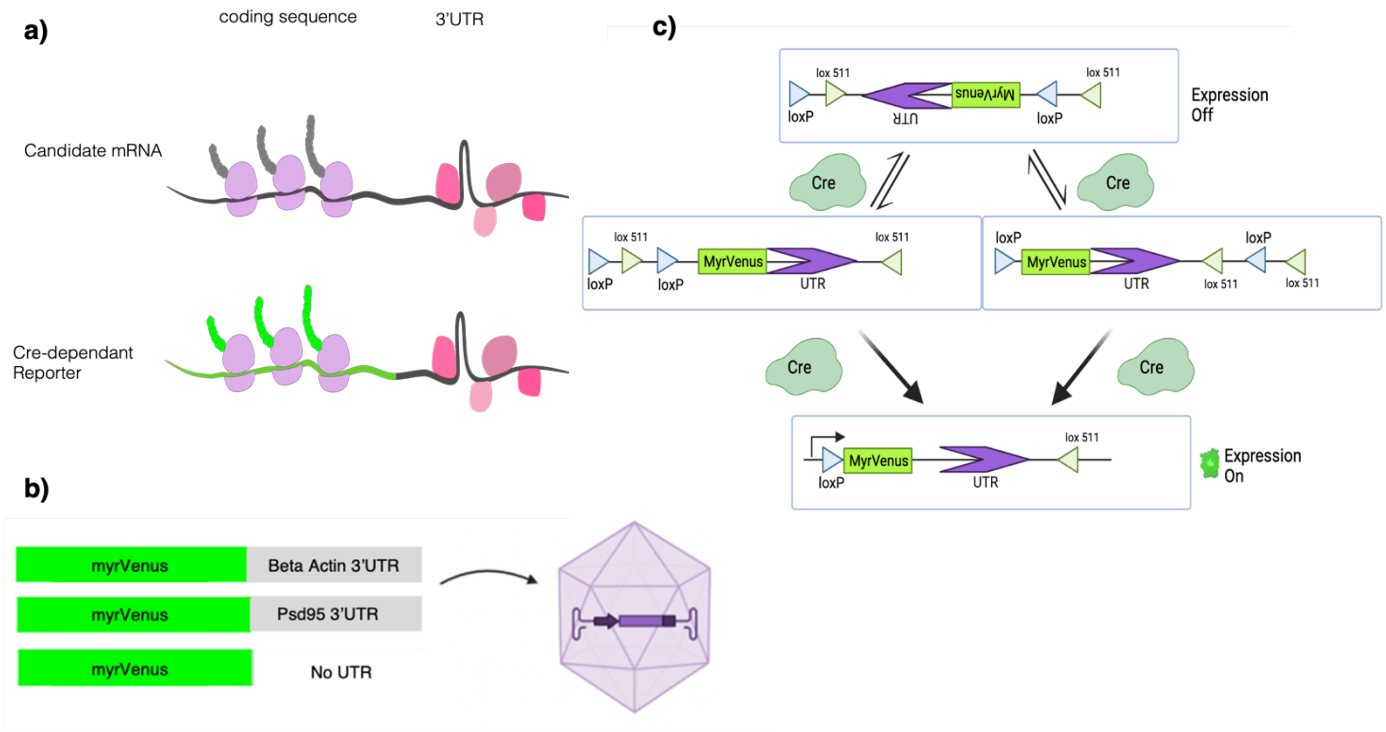

Fig. 1. Schematic representing our reporter constructs' architecture and conditional expression strategy. a) Figure adapted from Teresa Spanò showing the rationale for our reporters: the coding sequence of the candidate mRNA is replaced by that encoding venus, attached to the 3'UTR from the most abundantly localised mRNA variant of the gene of interest. b) Illustration of our two candidate reporters and a negative control that lacks a UTR sequence, which are packaged into AAVs c) Illustration of the flip-excision (FLEX) switch used to achieve conditional expression of our reporter constructs. Without Cre, the ORF is in an inverted configuration where the mRNA cannot be translated into protein. Conversely, in the presence of Cre, the mRNA is inverted, enabling the mRNA to be read out, localised, and the encoded protein to be synthesised.

1.5 Aim of the Project

To ensure that these reporters are valuable tools for measuring local translation, my project aim was to visualise the spatial distribution and expression of the mRNA encoding these constructs and compare them with their endogenous mRNA correlates. My research question was two-pronged. First, I was interested in whether *Beta Actin* and *Psd95* 3'UTRs drive the localisation of myrVenus mRNA into dendrites in cultured neurons. Second, I wanted to see whether the dendritic distribution of the reporter constructs is similar to that of endogenous *Beta Actin* and *Psd95* mRNA transcripts.

2. Methods

To evaluate whether the use of *Beta Actin* and *Psd95* 3'UTRs could directly localise myrVenus mRNA into dendrites in cultured neurons, RNA Fluorescence *in situ* Hybridization (RNA FISH) was used. This method relies on fluorescently labelled probes to detect specific RNA sequences[81]. For this project, RNA FISH was used to visualize venus reporters and their endogenous counterparts in neurons in culture.

2.1 Cell Culture

Dissociated rat cortical neuronal cultures were prepared from postnatal day 0 or 1 rat pups by plating neurons on poly-D-lysine–coated glass-bottom Petri dishes (MatTek) at a density of 40x 10^3 neurons/dish. The cultures were maintained in a growth medium (Neurobasal-A supplemented with B27 and GlutaMAX-1 from Life Technologies) at 37°C and 5% CO2 by Schuman lab technicians: Ina Bartnik, Nicole Fürst, Anja Staab, and Christina Thum.

2.2 Tissue Section Preparation

For tissue samples, mice brains used for the *in vivo* experiments where the reporters were previously injected into the auditory cortex were perfused, dissected, and sectioned on a vibratome or cryosectioned to achieve 40µm sections. These were then placed in phosphate-buffered saline (PBS) until used. Tissue samples were fixed in 4% paraformaldehyde in PBS for 20 min before starting the FISH protocol.

2.3 Drug Treatment

The puromycylation and subsequent PLA protocols were performed to detect newly synthesized proteins following tom Dieck et al. (2015)[15] methods. Drug treatments were performed as follows: for puromycin labelling experiments, cultured neurons transduced with the reporters *Beta actin UTR*, *Psd95 UTR,* and No UTR were treated with 10µM puromycin for 5min. For the protein synthesis inhibition controls, neurons were treated with 40µM anisomycin 45 min before puromycin addition. Each treatment occurred on the hot plate (40°C) until fixation, and neurons were individually returned to the incubator for the interim periods. A timed plan experiment was written out beforehand, and a timer was used to ensure the administration of anisomycin occurred precisely 45 minutes before the addition of puromycin.

2.4 Transduction and Cell Fixation

Cortical cultured neurons at DIV 9-13 were transduced with one of the myrVenus reporters or the no UTR control virus, together with a virus encoding Cre recombinase. After expressing the viruses for seven days, the neurons underwent two washes with phosphate-buffered saline (PBS) followed by fixation in 4% paraformaldehyde (PFA) in PBS for 20 min. They were then permeabilized with a proprietary panomics detergent for 5 min and washed 3x with PBS (Fig. 2 Step 1). Samples were then processed for FISH experiments (See 2.5: Fluorescence *in situ* Hybridization in Tissue/Culture). For the endogenous transcripts, neurons were not transduced but fixed and permeabilized as explained herein.

2.5 Fluorescence *In Situ* Hybridization in Culture/Tissue

For neurons in culture, ViewRNA ISH by Thermo Fisher detergent was applied for 5 min followed by 3 washes in phosphate-buffered saline (PBS). Next, target-specific *in situ* hybridization was performed using ViewRNA ISH by Thermo Fisher probes diluted 1:100 in probe set mixture for 3h at 40°C (Fig. 2 Step 2). A humidity chamber was created for all incubations at 40°C using wet towels and plastic wrap to prevent the neurons from drying out. Following probe hybridization, neurons were washed three times for 5 min each with a proprietary panomics wash buffer. These were then immediately processed for amplification.

Pre-amplification was performed with preAMP mixture (pre-amplification reagent diluted 1:25 in Hybridization buffer B) for 30 min at 40°C (Fig. 2 step 3). After pre-amplification, samples were washed with ViewRNA ISH by Thermo Fisher wash buffer 3x and amplification buffer was applied (amplification reagent diluted 1:25 in Hybridization buffer B) for 30 min at 40°C and then washed 3x in PBS, as outlined by (Fig. 2 step 4). Lastly, the labelling probes were applied for 30 min at 40°C (LP 1:25 in Hybridization buffer C (Fig. 2 step 5). Then, the neurons were washed 3x with a ViewRNA ISH by Thermo Fisher wash and 2x in PBS to be processed for immunofluorescence (IF) and subsequently imaged. The same FISH protocol was employed for tissue slices with the following amendments: the detergent was applied for 10 min, and the probe set mixture was applied overnight at 40°C in a humidity chamber. In addition, the incubation steps of the amplification process were 1h long instead of 30 min. Before being processed for IF, tissue samples were additionally fixed for 10 min in 4% PFA post *in situ* hybridization.

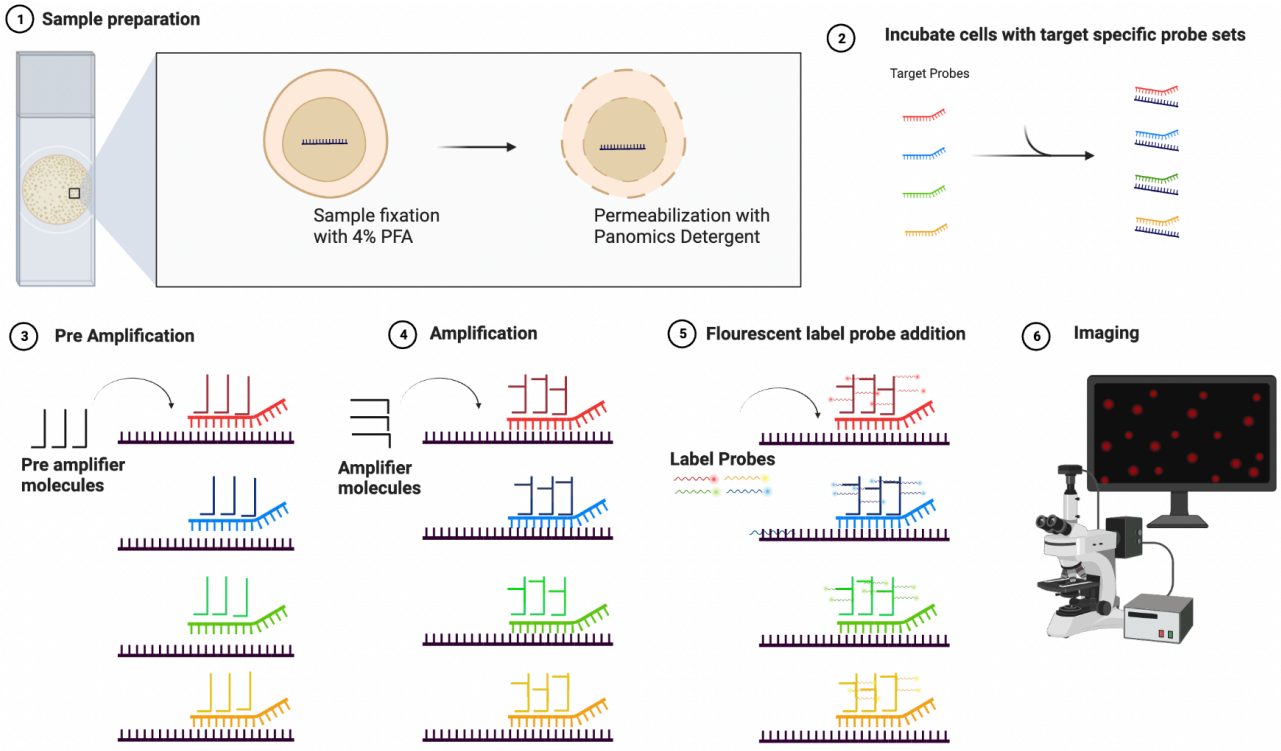

Fig. 2. Fluorescence in situ hybridization signal amplification pipeline, using the Thermo Fisher ViewRNA Cell plus assay[81]. 1) Prior to incubation, cortical cultured neurons (2-3 weeks old) were fixed with 4% PFA and permeabilized with a proprietary detergent. 2) Neurons are incubated in a humidity chamber at 40°C with target-specific oligonucleotide probe pairs, which bind adjacently to the RNA sequence. 3) The addition of pre-amplifier molecules ensures specificity by binding to pairs of probes on the target sequence rather than probes that may have bound separately. 4) Amplifier molecules hybridize with their corresponding pre-amplifier molecules creating a branched "tree" morphology. 5) In the last step of the amplification procedure, fluorescently conjugated oligonucleotide probes bind to the respective amplifier molecules resulting in an amplification of roughly 8,000- to 16,000-fold[81]. 6) After in situ hybridization, neurons are imaged with Zeiss LSM 880 confocal laser fluorescence microscope at 20x and 40x oil immersion objectives. Schematic created with BioRender.

2.6 Immunofluorescence

After FISH and immunostaining, cultured cortical neurons were blocked in 4% goat serum for 1h at room temperature. This was followed by overnight incubation with primary antibodies diluted in 4% goat serum at 4°C. Following overnight incubation, neurons were washed 5x for 5 min in PBS and incubated with secondary antibodies (diluted in 4% goat serum) overnight at 4°C or for 2h at 37°C. The secondary antibodies were washed off with five consecutive wash steps and stored in PBS or directly imaged. The tissue sections were blocked for 1h in 1% Triton, and 1% BSA in PBS at room temperature, and then incubated with primary antibodies in blocking buffer overnight, and secondary antibodies overnight at 4°C. Primary antibodies used for various experiments were guinea pig anti-map2 (SYSY; 1:1000), rabbit anti-NeuN (Abcam; 1:5000), chicken anti-GFP (Abcam 1:1000). Corresponding secondary antibodies were anti-guineapig Alexa 488 (1:1000), anti-chicken Alexa 488 (1:1000), anti-rabbit Alexa 568(1:1000), anti-guineapig Alexa 647(1:1000).

2.7 Image Acquisition

Confocal images were acquired with a Zeiss LSM 880 confocal laser fluorescence microscope using a 20x (test sets) or 40x oil immersion objective. The required wavelengths and lasers settings were adjusted in the manual setup. The images were taken with a 2048 x 2048-pixel resolution at 16-bit, with bidirectional scanning. For most experiments, 10 images were taken per dish at different positions (unless stated otherwise), the z-stack interval was set for optimal resolution and at each position, z-stacks were acquired spanning the entire depth of the neurons. Laser intensities and gain were kept the same within each imaging session, which consisted of all experimental conditions.

2.8 Image Analysis

After imaging, mRNA puncta were quantified and analysed using ImageJ, and z-stacks were condensed into maximum-intensity projections. Individual channels were separated, corresponding to the different fluorophores applied (with different wavelengths).

Binary images were created using the myrVenus channel thresholded with the Otsu method[82] (Fig. 3A). For one dendrite, an ROI was drawn manually with the segmented tool (60-pixel thickness and a minimum of 100µm length (Fig. 3B). This ROI was then used as an overlay on the RNA FISH channel (Fig. 3C). ROIs were then straightened; a binary mask was created using the FISH channel and a single erosion and dilation filter was applied to enhance the visualization of individual puncta (Fig. 3D).

Next, the 'analyze particles' tool was applied, which works by scanning the image or selection until the edge of an object is found. It then outlines the object using the wand tool, measures it, fills it to make it invisible, and resumes scanning until it reaches the end of the image or selection[83] (Figure 3E). Total puncta count and length of ROI (µm) were analysed. This process was repeated for 5 dendrites per imaged neuron. This means that for every soma, 5 dendrites were imaged. The soma was marked manually with the segmented tool and the 'analyze particles' function was applied using a similar pipeline. Subsequently, we also calculated the fractional distribution of the puncta in dendrites and somas, which provided a fractional account of the number of mRNA puncta in somas and dendrites over the total amount of puncta count of the ROIs. Statistical analysis and linear regressions were all performed using GraphPad Prism version 9.0.

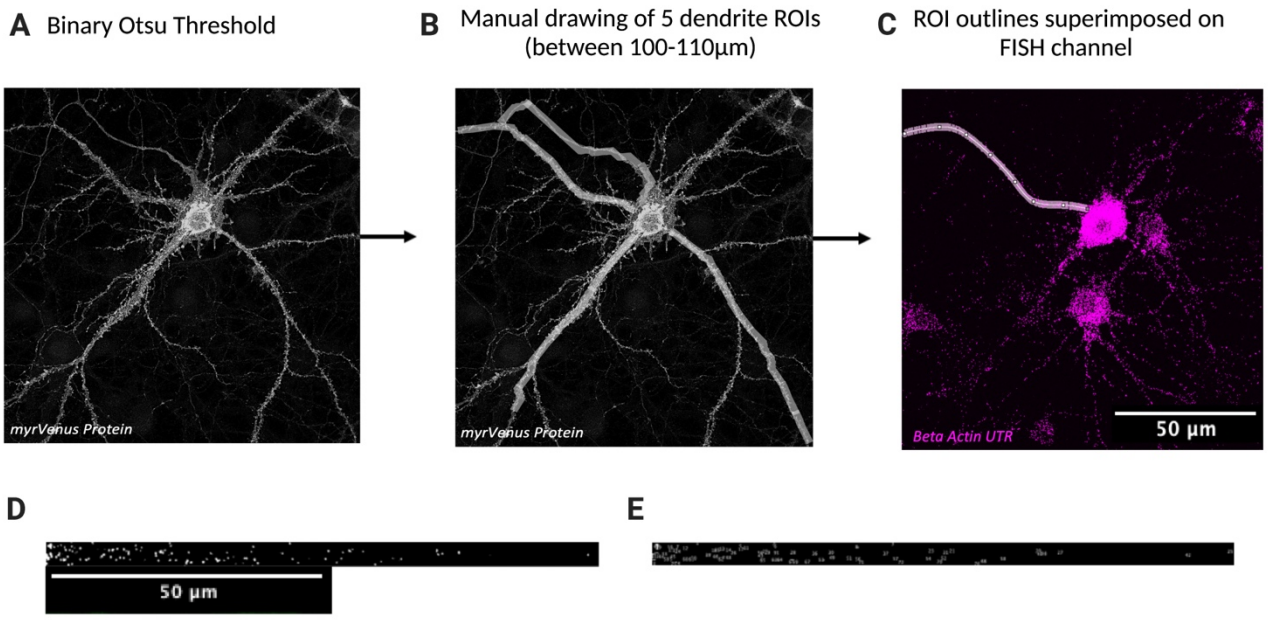

Fig. 3. Pipeline for dendritic puncta analysis with ImageJ (Version 2.3.0/1.53q). The representative confocal image (40x oil) shows FISH against the Beta Actin UTR reporter (scale bar 50µm). (A) Application of Otsu Threshold[82] to make a binary mask of the myrVenus protein channel. (B) ROIs were drawn between 100-110µm long and 60 pixels thick (scale bar 50µm). This process was repeated for 5 dendrite ROIs. (C) Selected ROIs were then used as an overlay on the RNA FISH channel. (D) ROIs were straightened, and a binary mask was created using the FISH channel. A single erosion and dilation filter was applied to enhance the individual puncta visualization. (E) The 'analyze particles' tool was applied, resulting in individual puncta counts for mRNAs in the dendrites.

2.9 Analysis of Puncta Across the Length of Dendrite

Dendrite ROIs from the image analysis were all plotted to ensure these were all between 100-110µm in length. If they were below this threshold, they were excluded from the analysis. In addition, the first 10µm of each ROI was omitted in the analysis to avoid potentially including puncta from the soma. The start of the dendrite was thus marked at 10µm into the ROI, and the puncta count was counted in 10µm bins for each dendrite. An average puncta count for each respective bin was created to yield the average raw puncta count for all the dendrite ROIs (n = 176 for the endogenous data sets and n = 169 for our reporter data set). For the fraction of total puncta, these same raw puncta were divided by the total amount of puncta in each dendrite to account for inherent differences in puncta and fluorescence signal within neurons and between replicates.

2.10 Puromycin-PLA

Puro-PLA was performed by Dr. Paul Donlin-Asp post-puromycylation. After the last permeabilization step in blocking buffer (0.5% Triton-x100 and 1% BSA in PBS) for 15 min at room temperature, neurons were blocked for 1h at room temperature in 4% goat serum in

PBS at room temperature. The following primary antibodies were applied with the stated dilutions overnight at 4°C in blocking buffer: mouse puromycin (Kerafast 1:3500), rabbit GFP (Abcam 1:500), and guinea pig Map2 (SYSY 1:1000). Rabbit PLAplus and mouse PLAminus secondary antibodies (Duolink reagents, sigma) were used as well as goat anti guineapig 488 (Abcam). Ligation and amplification mixtures were made according to the Duolink Detection reagents Red (Sigma) manufacturer's procedures.

First, neurons were washed 2-3x in PBS at room temperature. Secondary antibodies were applied in blocking buffer for 1h at 37°C in a humidity chamber. Next, neurons were washed 5x with buffer A (0.01 M Tris, 0.15 M NaCl, 0.05% Tween 20) at room temperature and a ligation mixture was applied for 30 min at 37°C in a humid chamber. Neurons were washed 3x with buffer A again at room temperature, and a amplification mixture with red/orange amplification stock was applied for 100 min at 37°C in a humidity chamber. Finally, neurons were washed 3x in buffer B (0.2 M Tris, 0.1 M NaCl) and 3x in PBS at room temperature and stored in PBS for a maximum of 24h before imaging. In parallel with puro-PLA, anti-Map2 immunostaining was performed to visualize dendrites.

3. Results

3.1 *In situ* Hybridisation of UTR Constructs and Endogenous mRNA in Culture

To assess the specificity of our FISH protocol, we used cultured cortical neurons transduced with the myrVenus reporter viruses. The specificity refers to the ability of the FISH probes to detect only the specific RNA sequence of interest, which in our case is the myrVenus reporter. In some cases, the probes could bind to sequences that are not of interest. Specifically, there was a chance the FISH probes would not distinguish between the myrVenus RNA and the RNA sequences present in the AAV genome, leading to non-specific hybridization events.

Using a Cre-dependent system, we could control whether the reporter's expression depended on the presence of the Cre-encoding virus. This confirmed whether the FISH signal observed came from the myrVenus reporter and not from other sources, such as endogenous mRNA. Furthermore, we stained for myrVenus protein as this was expected to only express in the presence of Cre, and Microtubule-associated protein 2 (MAP2) - a cytoskeletal protein that is highly expressed in dendrites and is, therefore, a reliable marker for these structures[84] – was used to visualise the dendritic arbours.

As expected, myrVenus mRNA (magenta) and myrVenus protein (yellow) were only detected with the co-addition of Cre (Fig. 4A), and we did not see any FISH signal in the absence of Cre (Fig. 4B). This showed that our FISH probes bound specifically, and that the reporter's expression was Cre-dependent. Moreover, mRNA puncta were detected in the cell bodies and dendrites of neurons.

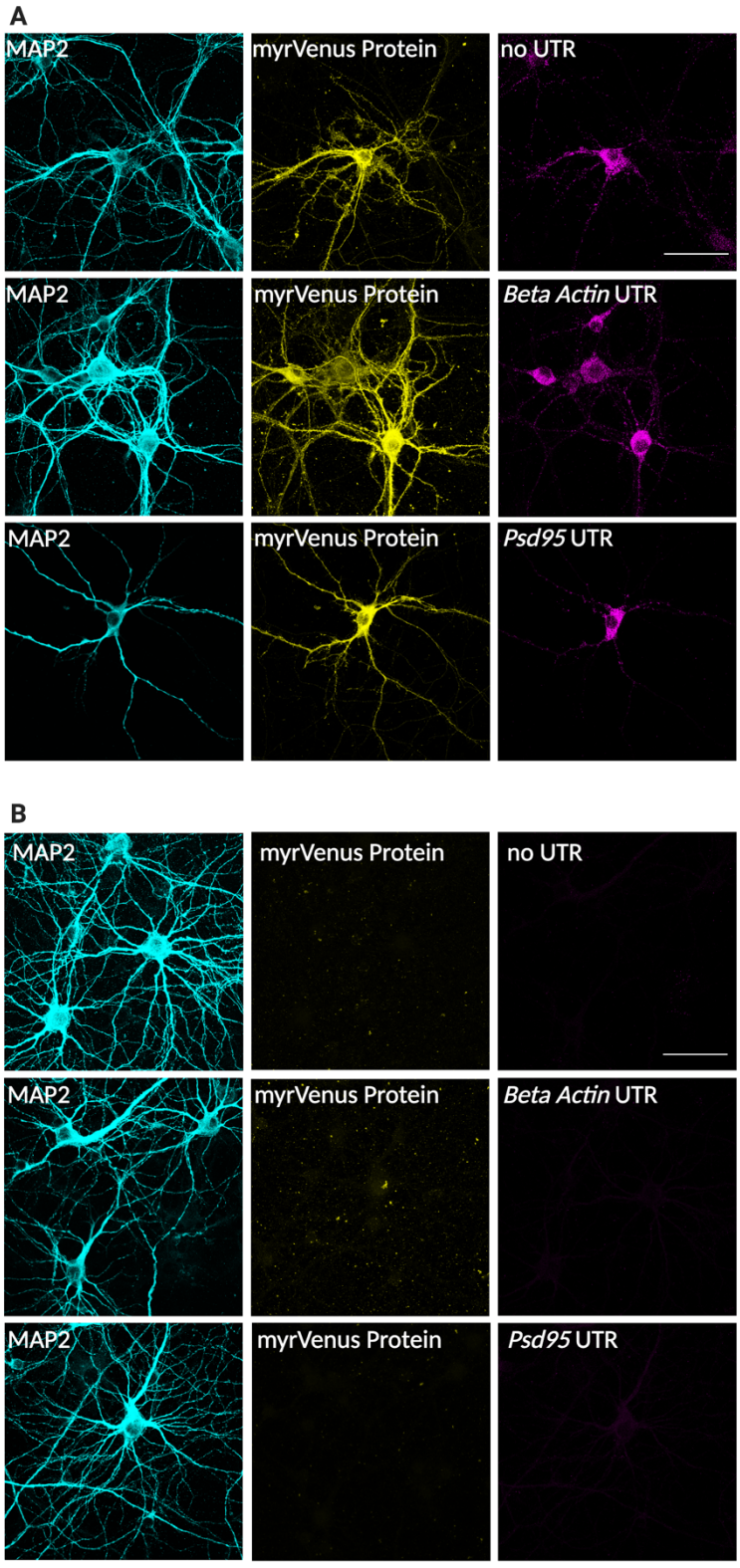

Fig. 4. Confocal images (40x oil) showing a FISH experiment in reporter-infected cultured cortical cells with and without Cre to control for probe fidelity and specificity. Additional staining for myrVenus protein (yellow) to visualize myrVenus expression with Cre and Map2 (cyan) was used to visualise the dendritic arbours. From top to bottom: No UTR, Beta Actin UTR, and Psd95 UTR constructs (scale bar 50µm). (A) shows cells co-infected with a virus encoding Cre recombinase and (B) indicates the controls without Cre. Only the upper panel shows a fluorescent signal, verifying that myrVenus protein and mRNA are expressed only when Cre is present. Figures created with BioRender.

Additionally, a control experiment was conducted where we assessed the FISH signal when adding and omitting the hybridization probe to confirm that the signal we observed was solely due to the probe binding with our mRNA of interest, which indeed was the case (Fig. 5). We concluded that the probe detection of myrVenus was specific and Cre-dependent.

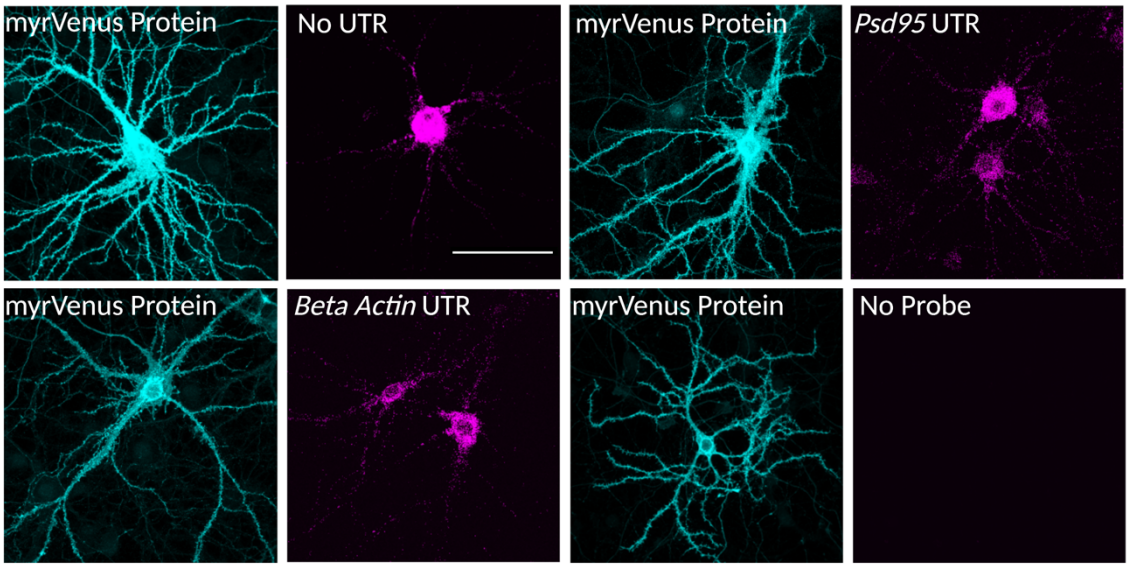

Fig. 5. Confocal images (40x oil) showing successful FISH experiment on cultured cortical cells transduced with our reporter Beta Actin UTR, Psd95 UTR, and no UTR control. From left to right, top to bottom: No UTR, Psd95 UTR, Beta Actin UTR, and a Beta Actin UTR no probe control (scale bar 50µm). Reporter constructs show a clear fluorescent signal, but no signal is seen for the no probe control. Figures created with BioRender.

After visualising these constructs, we next quantified how many of these mRNAs were localized in dendrites by employing two strategies. The first was to analyze the raw puncta count within 5 selected dendrites and the corresponding soma of each cell to see the variability between each data set. ImageJ was used to manually draw out 5 dendrite regions-of-interest (ROIs) of roughly 100µm in length, and the mRNA puncta within these were counted using the methods outlined in Methods section 2.8. The total for the five dendrites was combined to produce the dendrite compartment count for each cell.

Subsequently, the fractional distribution of the puncta in dendrites and somas was calculated. As described in the methods, this provided a fractional account of the number of mRNA puncta in somas and dendrites over the total amount of puncta of our dendrite and soma ROIs for each cell. This technique was implemented to normalize for potential variabilities seen in the raw puncta count, which was especially manifest in the reporter constructs. It would otherwise be an unfair comparison, as the lower overall puncta in endogenous mRNA led to lower dendritic puncta count relative to the reporter constructs.

To start, the lengths for each ROI were plotted to ensure that length would not be a confounding variable (Fig. 6A). If the ROI dendrite lengths were to be longer in one cell versus another one, there would be more area for mRNA puncta to be present, resulting in higher puncta count in that dendrite compared to the shorter dendrite, despite both having the same level of mRNA expression. With consistent lengths, a fair comparison could be made regarding the average number of mRNA in dendrites across constructs.

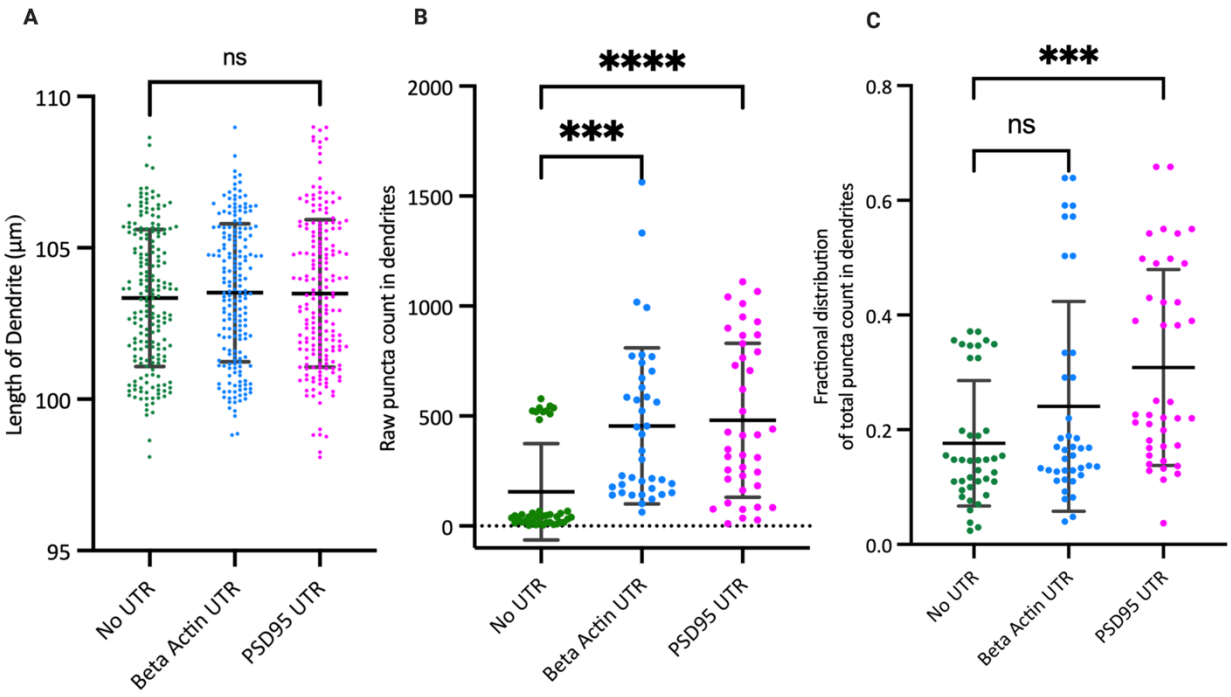

*Fig. 6. Analysis of puncta distribution for cortical cultured cells transduced with our reporter Beta Actin UTR and Psd95 UTR constructs and no UTR control. Four biological replicates, performed by Paul Donlin-Asp: 169 dendrites (each point showing five dendrites summed per cell) and 40 somas per construct (31 dendrites were omitted as they had lengths under 100µm). (A) Length analysis of reporter dendrite ROIs showing similar lengths (mean ± SD) for No UTR (103.3 ± 2.27µm), Beta Actin UTR (103.5 ± 2.28µm), and Psd95 UTR (103.5 ± 2.43µm). Differences in averages between constructs were not statistically significant as determined by ordinary one-way ANOVA with multiple comparisons test: F(2, 576) = 0.321, p = 0.726 (*P < 0.05; ***P < 0.001; ****P < 0.0001) (B) Graph showing raw puncta count (mean ± SD) for no UTR (155.6 ± 34.56), Beta Actin UTR (414.0 ± 48.64), and Psd95 UTR (469.3 ± 55.89). Differences in averages between constructs were statistically significant as determined by ordinary one-way ANOVA with multiple comparisons test F(2, 115) = 13.18, p = 0.0001, and post-hoc Tukey test; No UTR vs. Beta Actin UTR p-value 0.0001, No UTR vs Psd95 UTR p-value <0.0001 (C) Graph showing fractional distribution (mean ± SD) for no UTR (0.176 ± 0.110), Beta Actin UTR (0.241± 0.183), Psd95 UTR (0.308 ± 0.171). Differences in averages between no UTR and Psd95 UTR were statistically significant, but not between the no UTR and Beta UTR, as determined by one-way ANOVA: F(2, 115) = 7.00, p = 0.0013 and post-hoc Tukey test; No UTR vs. Beta Actin UTR p-value 0.1649, No UTR vs Psd95 UTR p-value <0.0008. Overall raw data shows an enrichment of the UTR-containing mRNA constructs in dendrites, signifying that these effectively localise to dendrites more than the no UTR construct. Analyses were performed with GraphPrism 9.*

The average length of dendrites was similar across all constructs as determined by the non-significant p-value of the one-way ANOVA analysis (p = 0.726). The ROIs with lengths lower than 100µm were omitted (31 dendrite ROIs out of the initial 200). We then looked at the distribution of mRNA in dendrites for our UTR constructs versus the no UTR control to see whether these were enriched (Fig. 6B). As shown, there was an enrichment of our UTR constructs in dendrites, which effectively localized to dendrites more than the no UTR construct. This was verified by the statistically significant p-value of the one-way ANOVA analysis (p = 0.0001) and post-hoc Tukey tests (No UTR vs Beta Actin UTR p-value 0.0001, No UTR vs Psd95 UTR p-value <0.0001). A similar enrichment was seen in the fractional distribution of puncta between constructs (Fig. 6C) as shown by the one-way ANOVA analysis (p = 0.0013). However, the post-hoc Tukey test revealed that this enrichment was only statistically significant for our *Psd95* construct. This is probably also attributed to the large standard deviation of *Beta Actin* since its mean fractional distribution (0.241) was higher than the no UTR (0.176). This matched our expectations, given that the UTR region contains the localisation motifs and would therefore have a higher dendritic localisation. After establishing that both reporters were enriched in dendrites, we wanted to see how this compared to the somatic puncta enrichment (Fig. 7).

The raw puncta count (Fig. 7A) in somas and dendrites of the no UTR, *Beta Actin* and *Psd95* constructs showed that there was a greater number of somatic puncta for our UTR constructs (*Beta Actin*: 2246.0 ± 1237, *Psd95*: 1692.0 ± 1201, no UTR: 1184.0 ± 1525). However, this was also due to the higher total raw count of the UTR constructs compared to the no UTR, due to their overexpression. Similarly, we saw a higher raw dendrite count for the UTR constructs compared to the no UTR (*Beta Actin*: 414.0 ± 307.6, *Psd95*: 469.3 ± 353.5, no UTR: 155.6 ± 218.6).

When observing the fractional soma to dendrite ratio (Fig. 7B) we observed similar values for our *Beta Actin* (0.761 ± 0.177 to 0.241 ± 0.183) and *Psd95* UTR constructs (0.692 ± 0.171 to 0.308 ± 0.171), and a higher somatic localisation for our no UTR construct (0.824 ± 0.101 to 0.241 ± 0.183). The variability between all three constructs was also comparable, as shown by the standard deviation values.

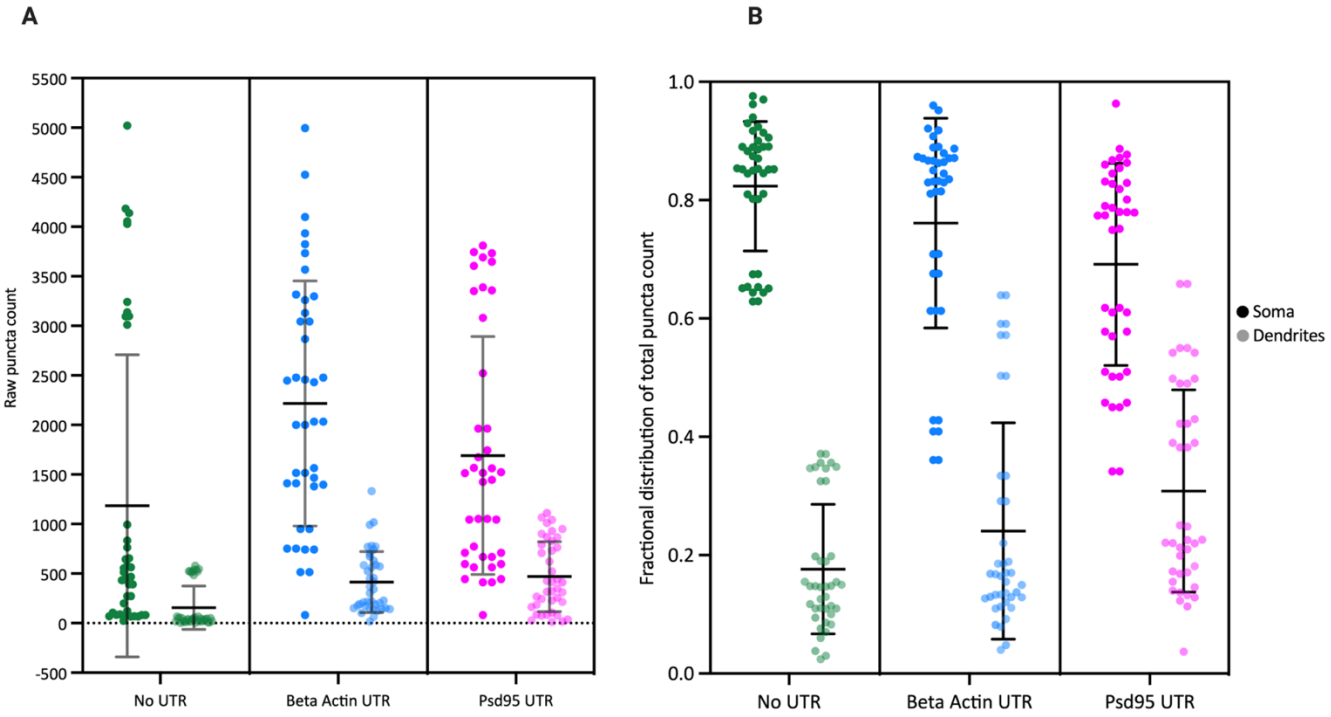

Fig. 7. Side-by-side comparison of puncta distribution in dendrites and their respective soma for cortical cultured cells transduced with our reporter Beta Actin UTR and Psd95 UTR constructs, and no UTR control (same data set and methods applied as Fig. 6). (A) Graph showing raw puncta count (Mean ± SD) with somas outlined by the darker circles (left side for each construct), and dendritic data points by the transparent circles (right side for each construct) for no UTR (soma: 1184.0 ± 1525, dendrite: 155.6 ± 218.6), Beta Actin UTR (soma: 2246.0 ± 1237, dendrites: 414.0 ± 307.6) and Psd95 UTR (soma: 1692.0 ± 1201, dendrites: 469.3 ± 353.5). (B) Graph showing fractional distribution (Mean ± SD) for no UTR (soma 0.824 ± 0.101, dendrites: 0.176 ± 0.110), Beta Actin UTR (soma: 0.761 ± 0.177, dendrites: 0.241 ± 0.183), Psd95 UTR (soma: 0.692 ± 0.171, dendrites: 0.308 ± 0.171). Analyses were performed with GraphPrism 9.

Next, we determined whether the reporter-infected constructs distributed similarly to the endogenous *Beta Actin* and *Psd95* mRNAs. By observing the distribution of endogenous *Beta Actin* and *Psd95* mRNAs, we not only got an insight into the innate behaviour and localisation of these mRNAs but also into how this localisation compared to our constructs. To answer the second part of the research aim, we analysed the distribution of endogenous *Beta Actin* and *Psd95* mRNA using the same FISH protocol, except in non-transfected cells and using probes against *Beta Actin* and *Psd95* rather than venus-encoding mRNA (Fig. 8). In addition, we analysed the expression of *CamKII* – an mRNA known to express strongly in neurons and robustly localise to dendrites – and *PolyA*, a ubiquitous sequence added on the 3' tail end of most mRNAs involved in their stability[11] and translation.

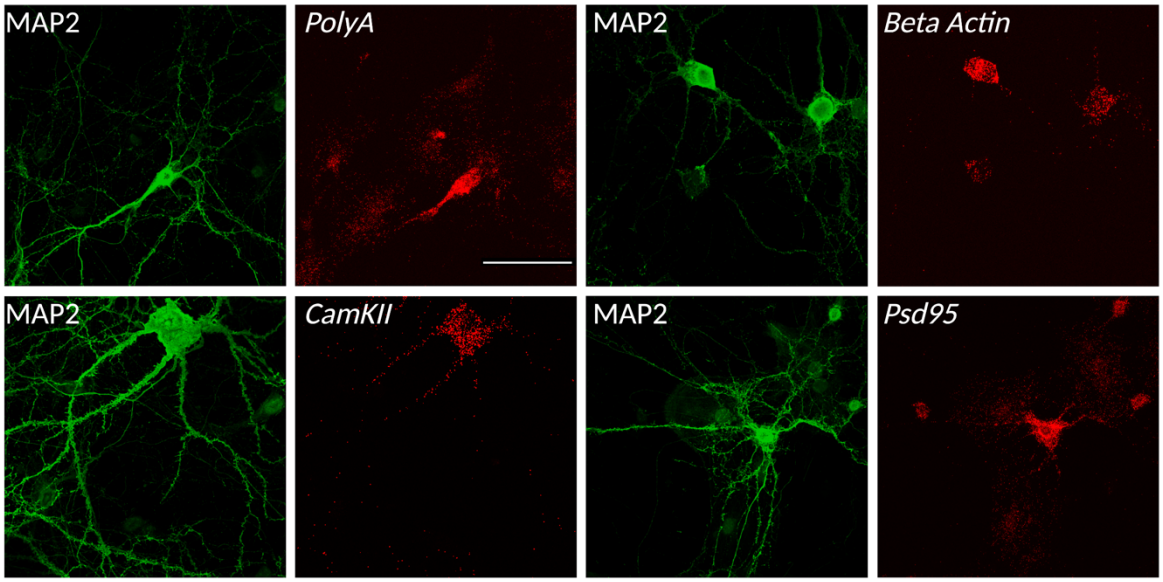

Fig. 8. Confocal images (40x oil) showing successful FISH experiments against endogenous candidate proteins in cultured cortical cells. In addition, FISH against CamKII and PolyA was conducted as a positive control since both are known to express robustly in dendrites. From left to right, top to bottom: PolyA, Beta Actin, CamKII, and Psd95 (red) and Map2 (green) outlining cells (scale bar 50µm). A clear fluorescent signal can be seen in dendrites and somas for all targeted mRNAs. Figures created with BioRender.

We noticed a clear punctate signal for both our UTR constructs and our positive controls *PolyA* and *CamkII*, and seemingly similar fluorescent intensity. After visualising the localisation and presence of our endogenous candidate mRNAs, we quantified this signal by counting the mRNA puncta in dendrites and somas. Puncta were counted using the methods outlined in the methods (2.8). We first ensured that the ROIs had a standardized dendritic length when counting the mRNA puncta to make an unbiased comparison between conditions. As with the reporter-infected cells, the same length analysis was performed (Fig. 9A) to ensure the ROIs drawn showed equal averages (100-110µm), which was the case. ROIs under 100µm were omitted from the subsequent analysis (24 dendrite ROIs out of the initial 200). We observed the mean raw dendritic puncta count of endogenous *CamKII* (639.1 ± 399.4) and *PolyA* (553.2 ± 139.7) and found that these localized in dendrites at a higher level than *Beta Actin* (189.9 ± 89.05) and *Psd95* (160.6 ± 38.47), as expected (Fig. 9B). However, given that our positive controls also had a greater somatic raw count, we again looked at the fractional distribution (Fig. 9C), to see whether these differences were consistent when normalizing for the total raw count of each mRNA. Indeed, *CamKII* (0.234 ± 0.118) and *PolyA* (0.263 ± 0.06) still showed a higher dendritic distribution compared to *Beta Actin* (0.183 ± 0.09) and *Psd95* (0.122 ± 0.04). This was also reflected by post-hoc Tukey tests showing significant differences between our UTR constructs and positive controls, but not between the positive controls themselves (See supplemental Fig. S1).

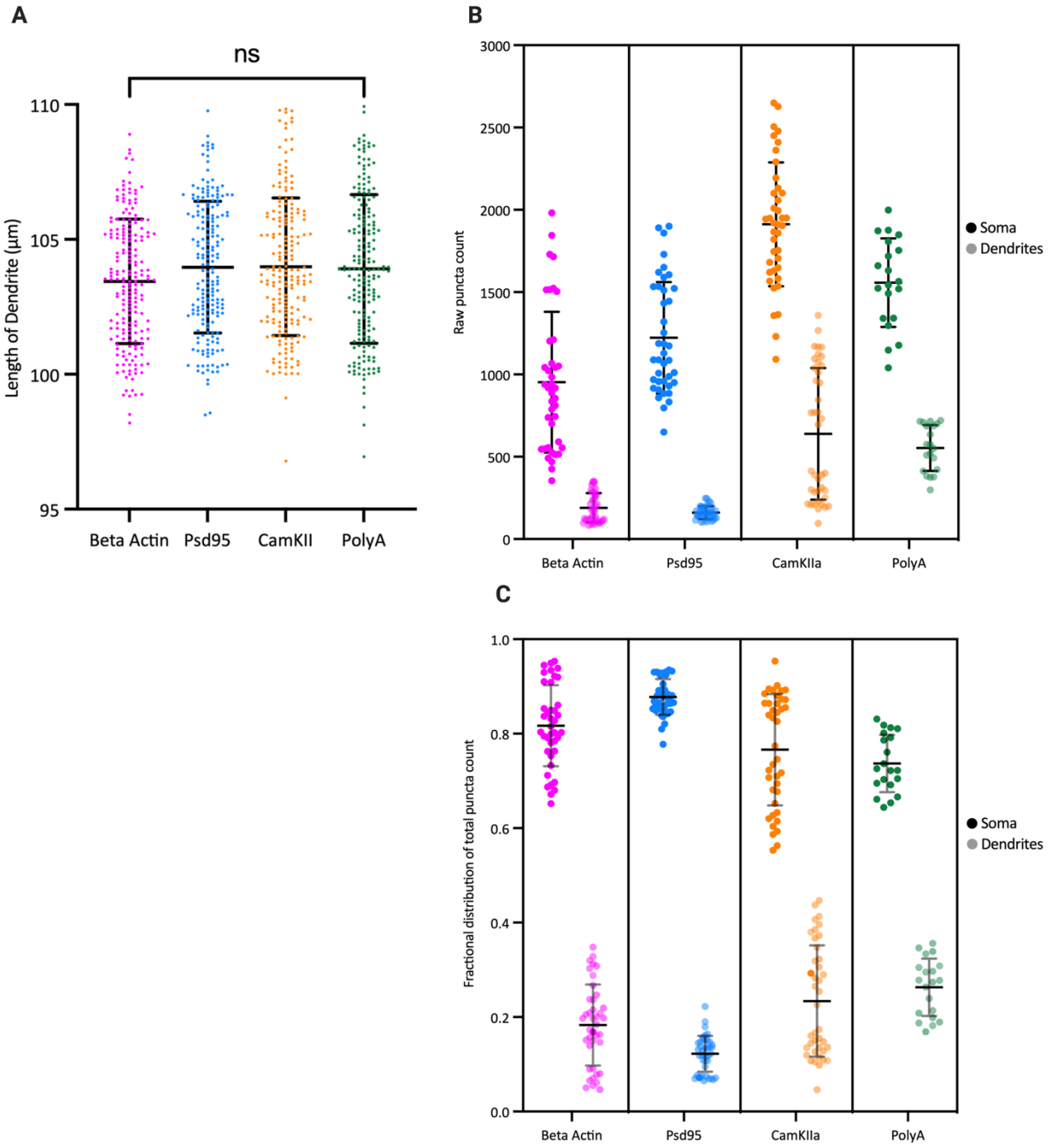

*Fig. 9. (A) Length analysis of dendrite ROIs (mean ± SD) for endogenous Beta Actin (103.3 ± 2.30µm), Psd95 (103.8 ± 2.43µm), CamKII (104.8 ± 2.84µm), and PolyA (105.3 ± 2.80 µm), showing similar mean lengths for all dendritic ROIs. Three biological replicates, and two technical replicates were performed by Dr. Paul Donlin-Asp: 176 dendrites (24 dendrites were omitted as they had lengths under 100µm). Differences in averages between constructs were not statistically significant as determined by ordinary one-way ANOVA with multiple comparisons test: F(3, 776) = 2.038, p = 0.107 (*P < 0.05; ***P < 0.001; ****P < 0.0001). (B) Analysis of raw puncta count (mean ± SD) for endogenous Beta Actin (soma: 953.2 ± 427.5 dendrites: 189.9 ± 89.05), Psd95 (soma: 1223 ± 339.0, dendrites: 160.6 ± 38.47), CamKII (soma: 1912.2 ± 375.9, dendrites: 639.1 ± 399.4), and PolyA (soma: 1558.0 ± 268.6, dendrites: 553.2 ± 139.7) in cortical cultured cells for the same data set. (C) Graph showing fractional distribution (mean ± SD) for Beta Actin (soma: 0.817 ± 0.09, dendrites: 0.183 ± 0.09), and Psd95 (soma: 0.878 ± 0.04, dendrites: 0.122 ± 0.04), CamkII (soma: 0.766 ± 0.118, dendrites: 0.234 ± 0.118), PolyA (soma: 0.737 ± 0.06, dendrites: 0.263 ± 0.06). Somas are outlined by the darker circles (left side for each construct), and dendritic data points by the transparent circles (right side for each construct). Similar fractional distribution is seen for Beta Actin and Psd95, whereas CamKII and PolyA showed a higher dendritic localisation.*

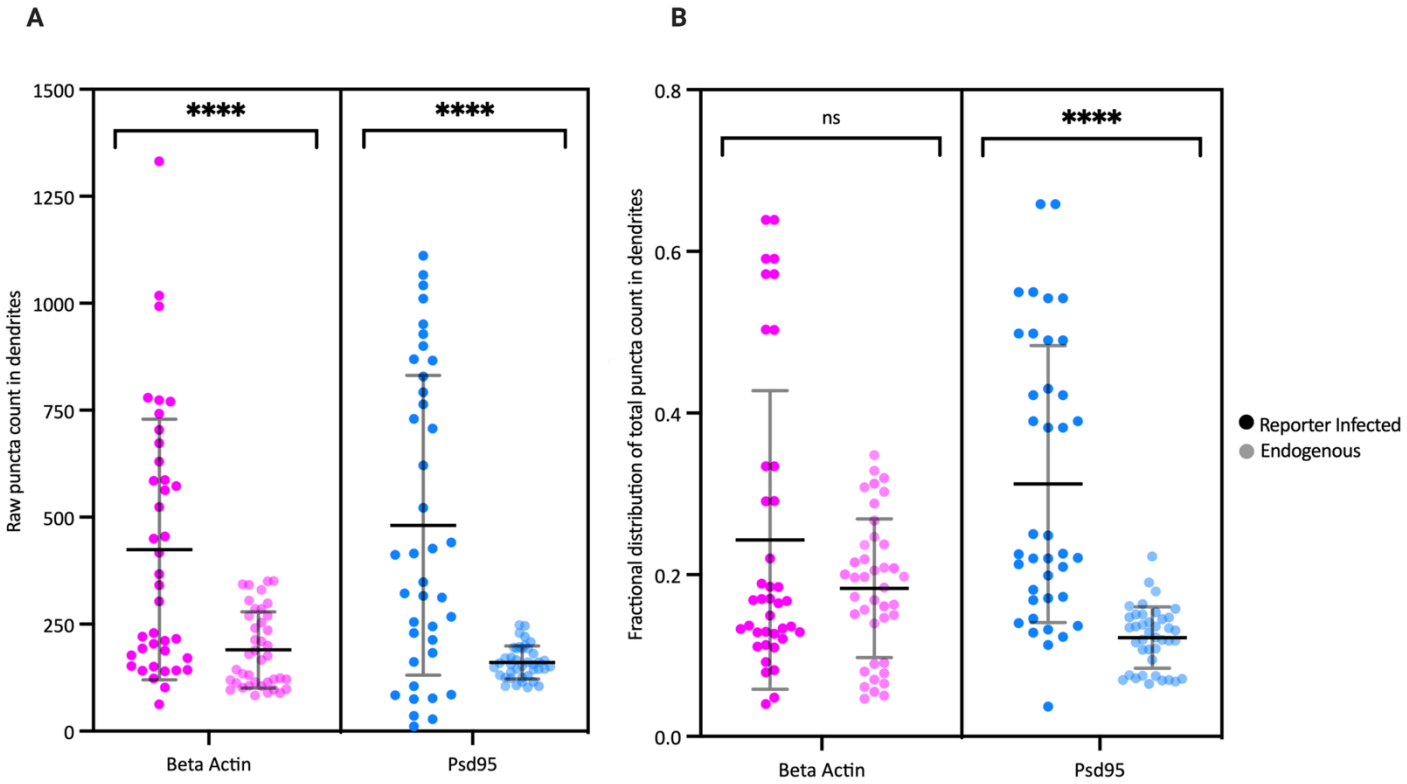

*Fig. 10. Analysis of puncta distribution in dendrites for the same data as Fig. 8-10. (A) Figure showing raw puncta count (mean ± SD) in dendrites for reporter infected (solid data points left side) and endogenous (transparent data points right side) Beta Actin (reporter-infected: 424.4 ± 304.6, endogenous: 189.9 ± 89.1) and Psd95 (reporter-infected: 480.9 ± 350.2, endogenous: 160.6 ± 38.47). Statistical significance bars indicate a two-tailed unpaired T-test (*P < 0.05; **P < 0.01; ****P < 0.0001). T-test shows significant differences between the raw counts of our reporter-infected constructs and endogenous mRNA, with the former showing much higher means. (B) Figure showing the fractional distribution of total puncta count (Mean ± SD) in dendrites for reporter infected (solid data points) and endogenous (transparent data points) Beta Actin (reporter-infected: 0.243 ± 0.185, endogenous: 0.183 ± 0.09) and Psd95 (reporter-infected: 0.312 ± 0.171, endogenous: 0.122 ± 0.04). Statistical significance bars indicate a two-tailed unpaired T-test (*P < 0.05; **P < 0.01; ****P < 0.0001). T-test shows non-significant differences between the fractional distribution of our reporter Beta Actin and endogenous Beta Actin mRNA (p-value 0.0893), but a statistical difference between endogenous and reporter Psd95. Reporter-infected cells show a greater fractional dendritic localization, but this difference is reduced compared to the raw counts. Analyses were performed with GraphPrism 9.*

Next, we compared the endogenous mRNA with our reporter mRNA data sets (Fig. 10). We can appreciate two things from the results. For one, the reporters show higher mean raw puncta count in the dendrites than the endogenous mRNAs (Fig. 10A). This difference was statistically significant as determined by a two-tailed unpaired T-test. Second, the reporter UTRs were expressed with greater variability than their endogenous mRNA counterparts. The first observation suggests that the reporter constructs may be more efficient at directing mRNA localisation into the dendrites than endogenous mRNA. However, as mentioned previously, our reporter constructs were overexpressed; therefore, the raw puncta count was greater overall.

Secondly, the reporter UTRs showed an overall greater variability than the endogenous mRNA data, as evidenced by the standard deviation values for the raw count and fractional distribution. This might indicate that the reporters are affected by other factors influencing their localization and stability within the dendrites, which will be outlined in the discussion.

Lastly, we observed a similar fractional distribution (Fig. 10B) between endogenous *Beta Actin* (0.817 ± 0.09 and 0.183 ± 0.09, respectively) and *Psd95* (0.878 ± 0.04 and 0.122 ± 0.04, respectively) as our reporter constructs *Beta Actin* (0.761 ± 0.177 and 0.241± 0.183 respectively) and *Psd95* (0.692 ± 0.171, and: 0.308 ± 0.171 respectively). Notably, the dendritic distribution was slightly lower for the endogenous mRNA. Again, this is most likely attributed to the lower mean raw count (Fig. 10A). The two-tailed unpaired T-test analysis showed that the difference between endogenous and our reporter *Beta Actin* was insignificant, but that for *Psd95*, it was. An explanation for why our *Beta Actin* constructs behave more similarly to their endogenous counterparts could lie with the higher expression fidelity of the *Psd95* virus resulting in a higher mRNA count.

3.2 Analysis of mRNA Distribution Across Dendrite Lengths

After confirming that our reporter constructs were localised in dendrites and behaved similarly to the corresponding endogenous mRNA, we investigated their distribution in dendrites. Given that *Beta Actin* UTR and *Psd95* UTR were expressed to a much greater extent (as demonstrated by the higher total raw count in culture Fig. 10), we wanted to determine if these reporter constructs have a similar distribution along dendrites as their corresponding endogenous correlates.

To answer our question, dendrite ROIs from previous data sets were utilized in the analysis. The average length of these ROIs ranged between 100-110µm (Fig. 6A and 9A), and those shorter than 100µm were excluded from analyses. This enabled a fair comparison of mRNA spatial distribution between constructs. The initial 10µm of each ROI was excluded from the analysis to avoid the potential inclusion of puncta from the soma. The start of the dendrite was thus marked at 10µm into the ROI, and the puncta count was recorded in 10µm increments along each dendrite. An average puncta count for each bin was calculated to produce the average raw puncta count across all dendrite ROIs (n=167 for reporter-infected data sets, 176 dendrites for the endogenous data set). The fraction of total puncta was determined by dividing the raw puncta count by the total puncta count in each dendrite to account for variability in puncta and fluorescence signal among cells and between replicates (Methods 2.9).

Our analysis revealed that most of the total puncta (Fig. 11) were located within the first 30µm of the dendrite, with a decrease in puncta across dendrite length for both endogenous mRNA (Fig. 11A-B) and the reporter *Beta Actin* and *Psd95* constructs (Fig. 11C-D). Fig. 11C shows that beyond 20µm, the number of mRNA puncta per bin for the no UTR construct was less than 5, significantly lower than the reporter constructs containing a UTR sequence. Additionally, the distribution of our reporter constructs (Fig. 11C-D) closely resembled that of their endogenous counterparts (Fig. 11A-B), accurately reflecting the distribution of *Beta Actin* and *Psd95* in physiological conditions. A linear regression model was fit to the data using GraphPad Prism, as this was the simplest method to analyze the line coefficients when comparing the datasets.

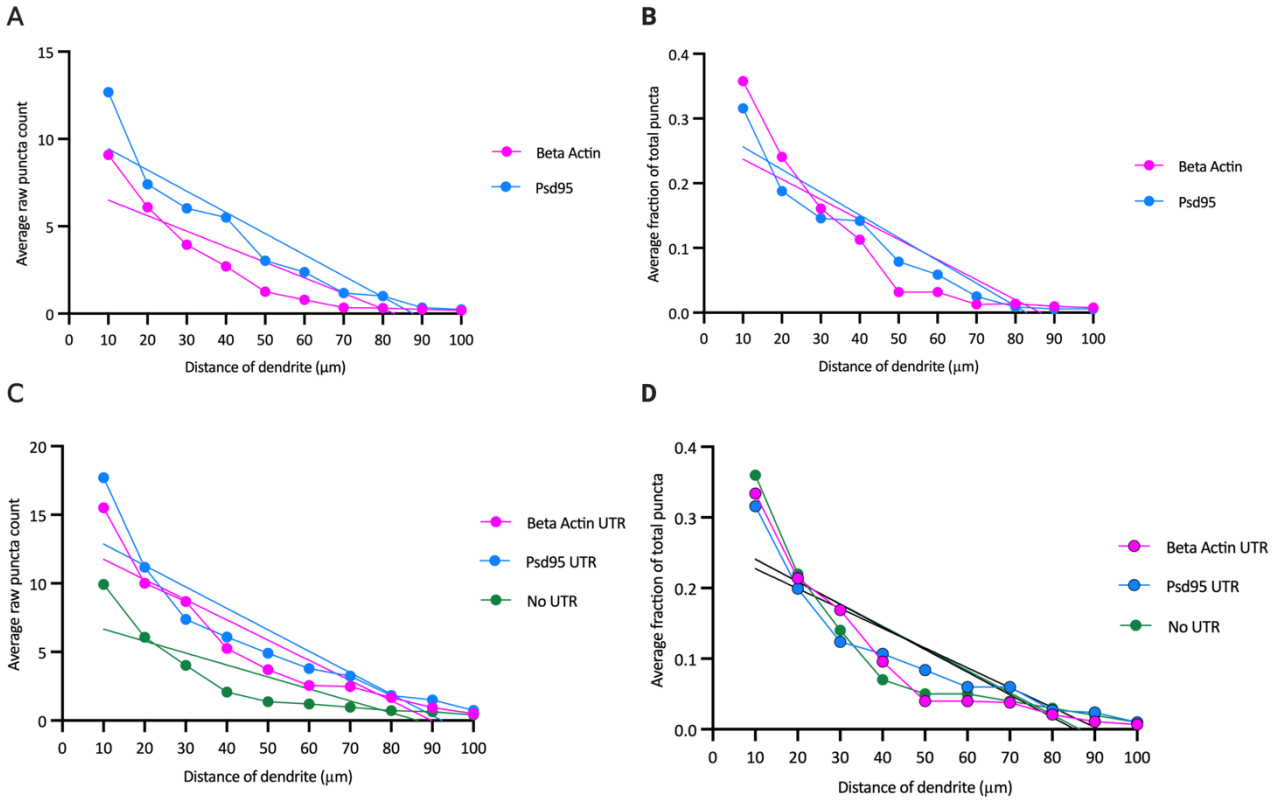

Fig. 11. Analysis of puncta distribution of dendrite ROIs from the same endogenous mRNA and reporter infected data sets as in Fig 7-11. The puncta for each dendrite ROI (All 100-110µm in length) were binned in 10µm increments. To ensure that the overlap between the somatic region and the start of the dendrite was clearly distinguished, the first 10µm of the ROIs were excluded. (A) Raw count and (B) fractional puncta distribution for endogenous Beta Actin (Magenta) and Psd95 (Blue). A simple linear regression was calculated with GraphPad Prism. The slope coefficients tell us the relative puncta signal distribution from the soma across the dendrite; a higher negative coefficient indicates that puncta concentrate close to the soma, and vice versa. Linear regression for (A) Beta Actin: $-0.08896 * X + 7.390$ *and Psd95:* $-0.1213 * X + 10.65$ *and (B) Beta Actin:* $-0.003516 * X + 0.2916$ *and Psd95:* $-0.003103 * X + 0.2683$ *(C) Raw count and (D) fractional puncta distribution for reporter infected Beta Actin UTR (magenta), Psd95 UTR (blue) and no UTR (green). Linear regression for (C) Beta Actin UTR:* $-0.1472 * X + 13.23$*, Psd95 UTR:* $-0.1563 * X + 14.43$ *, no UTR:* $-0.08710 * X + 7.535$ *and (D) Beta Actin UTR:* $-0.003199 * X + 0.2729$*, Psd95 UTR:* $-0.002805 * X + 0.2554$*, no UTR:*$-0.003145 * X + 0.2720$.

The linear regressions (Fig. 11A, 11C) show similar slope coefficients for all constructs: *Beta Actin*: -0.089 vs *Beta Actin* UTR: -0.147 and *Psd95*: -0.121 vs *Psd95* UTR: -0.156. As previously demonstrated, the reporters express at a higher level than the endogenous mRNAs, which could affect the models. Therefore, we also compared the fractional distribution of puncta along dendrite length for all constructs with their respective best-fit lines (Fig. 12). The slope coefficients of our reporter and endogenous *Beta Actin* and *Psd95* were very similar: -0.0035 endogenous *Beta Actin* (purple), -0.0031 endogenous *Psd95* (orange), -0.0032, *Beta Actin* UTR (magenta) and -0.0028 *Psd95* UTR (blue). This demonstrates that our reporters distribute comparably to endogenous mRNA in dendrites of 100µm.

Our experimental results align with the theoretical predictions of Fonkeu et al. (2019)[85] regarding the distribution of mRNA in dendrites. Their paper provides a dynamic computational prediction for the spatial arrangement of mRNAs and proteins in dendrites. The equation is based on established values for passive diffusion, active transport, and degradation rates of mRNAs found in the literature. It also considers the possibility of local translation of mRNA molecules at synapses, variations in translation rates along the dendrite, and different degradation or sequestration rates along the dendrite. The model was assessed using endogenous *CamKIIa in vitro*, and the experimental data fell within the proposed theoretical boundaries.

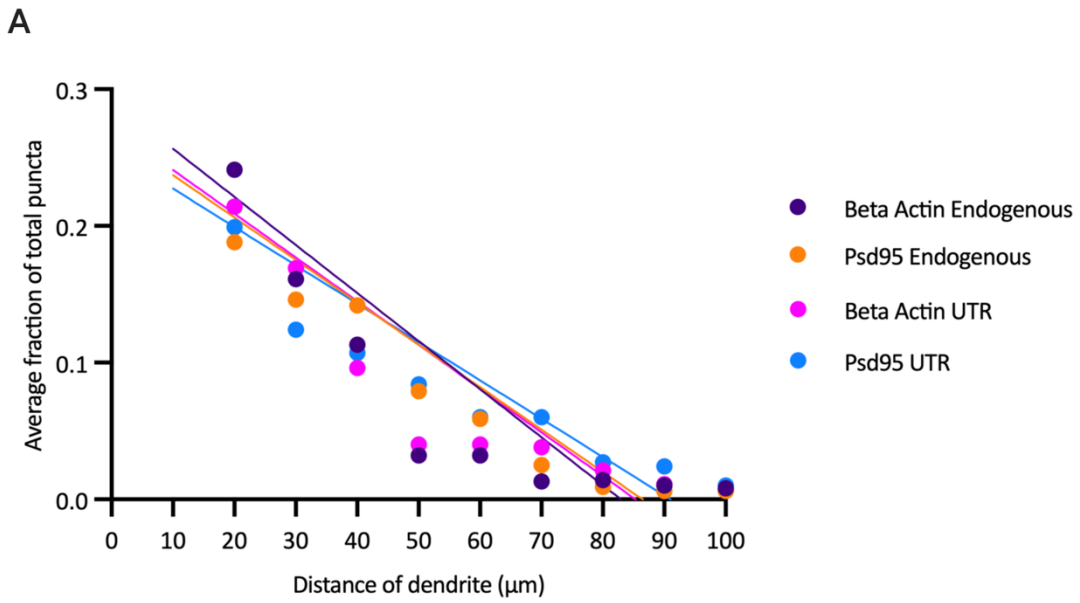

Fig. 12. Side-by-side analysis of fractional puncta distribution for endogenous Beta Actin and Psd95 and reporter Beta Actin and Psd95 UTR is shown in Fig. 12B-D. Slope coefficients for lines of best fit in descending order: -0.0035 endogenous Beta Actin (purple), -0.0031 endogenous Psd95 (orange), -0.0032 reporter Beta Actin (magenta) and -0.0028 reporter Psd95 (blue). As shown by the similar, if not equal slope coefficients, the distribution of puncta across the dendrite length is homogenous for both endogenous and reporter constructs: most puncta accumulate near the beginning of the dendrite and decrease incrementally towards the distal end of the dendrite.

3.3 *In situ* Hybridization of Our Reporter Constructs and Endogenous mRNA in Tissue

Our experiments in cultured cells (3.1) demonstrated that our reporter constructs were localised in dendrites and behaved similarly to endogenous mRNA. Furthermore, we observed that the distribution of both reporter and endogenous mRNAs decreased with increasing dendrite length (3.2), which aligns with previous research findings by Fonkeu et al.[85]. Next, we wanted to analyze whether what we saw in culture was mirrored in tissue samples. For the experiments of Dr. Paul Donlin-Asp and Teresa Spanò, our mRNA constructs were unilaterally expressed in the auditory cortex of mice and imaged *in vivo*. After this, brains were perfused, sliced, and processed for FISH against myrVenus, to see whether our reporters were localising in dendrites *in vivo*.

The FISH probes were initially evaluated and optimized to ensure that we could reliably and accurately detect myrVenus in tissue (Figure 14). We performed imaging on experimental and control cortical hemispheres, where one side was injected with the reporter virus and the cre-encoding virus, while the other was not. This approach was utilized to evaluate the signal-to-noise ratio and specificity of the FISH probes on complex tissue. The non-injected hemisphere served as a control, as the neurons in this area were not infected with either virus. Thus, any observed signal in this region could be attributed to background noise rather than the reporter's presence.

In ideal circumstances, the myrVenus FISH puncta should only be visible in dendrites that contain myrVenus protein. The slices were stained for myrVenus protein to differentiate between any possible background noise by comparing the injected and non-injected cortex as described. In tissue, the background noise can be caused by different factors, such as the probes non-specifically binding to other RNA or hybridizing to the viral genome. If a signal were to be present in the negative controls that lacked our mRNA reporter, it is likely that the FISH probes were not specific to the target sequence and instead were binding to other similar sequences. However, our previous work in cultured neurons suggested that would not be the case (Fig. 4).

Our results showed that the non-injected side of the cortical hemisphere had significantly less signal than the injected hemisphere (Fig.13). This is consistent with the probes being specific and not binding to other non-target RNAs. However, when comparing the myrVenus protein

and myrVenus mRNA images in the injected hemisphere, we noticed FISH signal in the latter that did not correspond to the dendritic outline produced by the myrVenus protein. This dendrite signal was therefore most likely originating from the AAV reporter itself, as it was only found in the injected hemisphere, suggesting that the FISH probes were binding to the reporter DNA in addition to or instead of the target mRNA of the AAV. Due to the inability to distinguish between viral RNA and DNA, it was impossible to determine if the signal seen was from localised mRNA or a copy of the AAV. Consequently, the location of the reporter mRNA could not be evaluated using FISH.

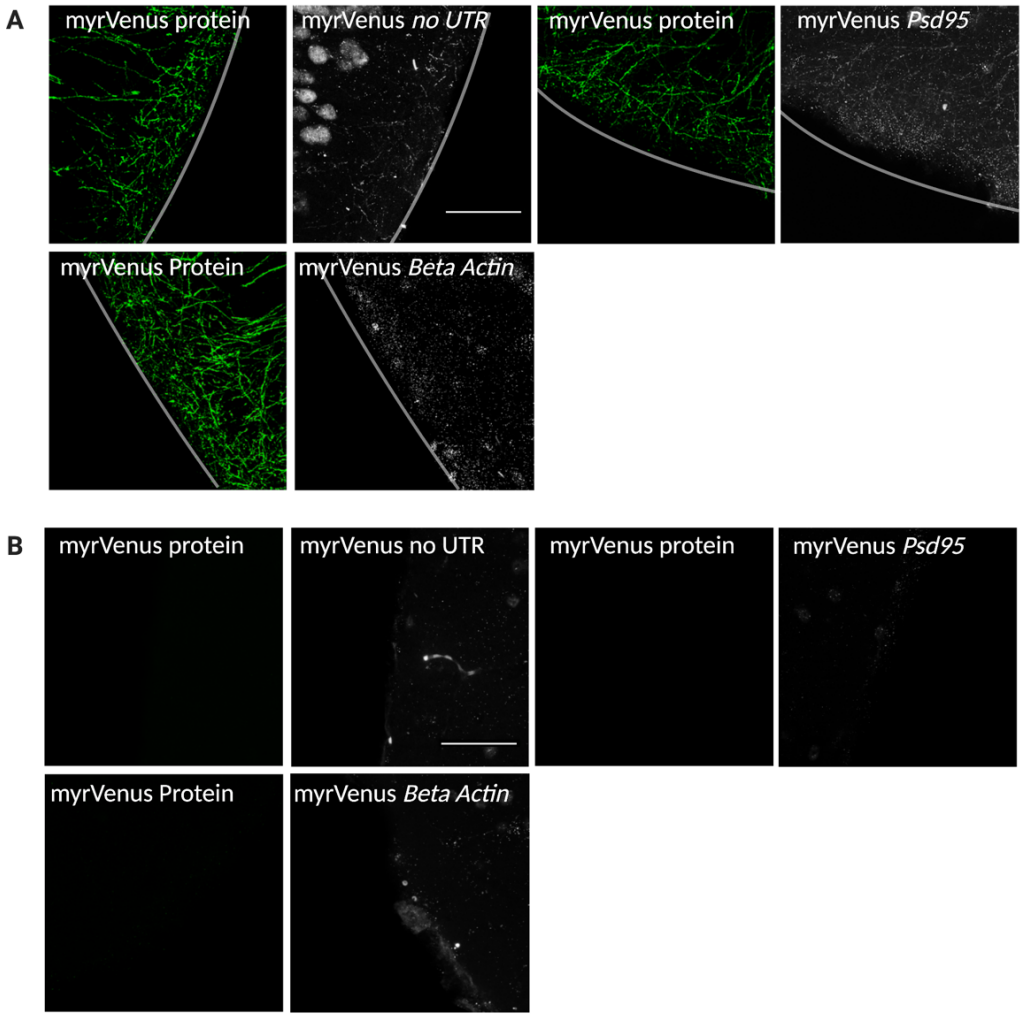

Fig. 13. Confocal images (40x oil) showing (A) FISH on reporter infected 40um auditory cortex slices and (B) cortex slices without reporter injection for the no UTR, Beta Actin UTR, and PSD95 UTR constructs, respectively (Scale bar 50µm). Transparent white lines show manually drawn outlines of the outer auditory cortex boundary. yrVenus protein (green) shows dendrite outlines on the auditory cortex's outer edge. In the cortical side injected with our reporters, we see a clear expression of myrVenus protein (green). In addition, a punctate signal is seen for the no UTR, Psd95, and Beta Actin myrVenus constructs. Some background noise for myrVenus mRNA is visible in all constructs, as the signal falls outside the boundaries of the myrVenus protein. In the side of the hemisphere without injection of AAVs or Cre, we see an absence of fluorescent signal for myrVenus protein or the reporter mRNA.

Despite the difficulty in separating mRNA from the viral genome in slices, the location of these mRNAs in dendrites was successfully confirmed *in vitro*. In light of this, Dr. Paul Donlin-Asp and Teresa Spanò continued exploring alternative detection strategies while the focus shifted to determining if the endogenous mRNA for *Beta Actin* and *Psd95* could be identified and localised to layer 1 of the auditory cortex. While we were aware that over-expression could lead to localisation of the reporters, through visualization of the endogenous mRNAs, we could examine the potential impact of endogenous *Beta Actin* and *Psd95* mRNA translation in layer I – where their subsequent translation would be utilized during learning and memory.

To answer this question, we performed FISH against our endogenous *Psd95* and *Beta Actin* (Fig. 14A-B). Additionally, myrVenus protein and neuronal nuclear protein NeuN[86] were stained to distinguish the boundaries of layer I. Panels A and B show a clear FISH signal for endogenous *Psd95* and *Beta Actin*. Since *Beta Actin* is known to be present in glial cells and interneurons[87], we would expect strong, condensed patches of signal in layer I representing these areas, as well as signal from axons and dendrites projecting from deeper layers. In addition, a large amount of the signal was somatic for *Beta Actin* in layer I; but we could still detect puncta likely originating from dendrites or axons.

As a positive control, we tested *Poly A* since the poly(A) tail is present in almost all mRNA, and it can be used as a universal marker for mRNA in FISH experiments[45]. Our results showed a bulk mRNA detection with the polyA probe. We also examined negative controls for *PolyA* and *Psd95* by using *PolyT* and *Psd95* sense strands and hybridizing them with anti-sense probes. These showed no robust FISH signal as expected (Fig. 14C), since these contained the reverse complementary sequence of their *PolyA* and *Psd95* antisense counterparts. To summarize, our findings indicated the presence of the endogenous mRNAs of interest in layer 1, and that our negative controls worked robustly.

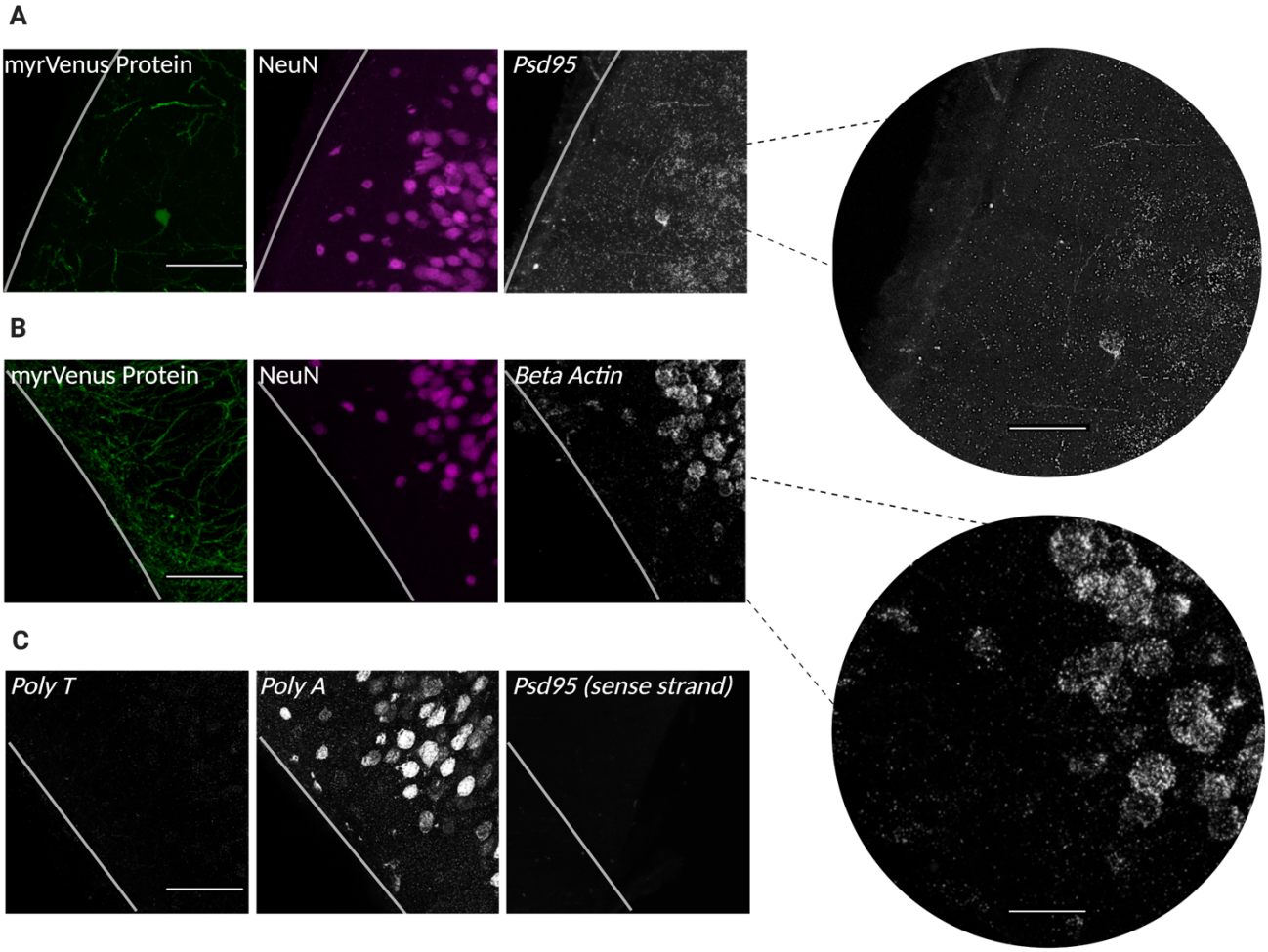

Fig. 14. Confocal images (40x oil) showing FISH on endogenous mRNA in 40µm auditory cortex slices. (A) show representative FISH images for Psd95 (white) and (B) Beta Actin (white) with additional staining against myrVenus protein (green) to ensure that we were observing cortical layer I, and NeuN (magenta) to outline cell bodies (Scale bar 50µm). Zoomed-in (2.5x) panels show individual puncta for Beta Actin and Psd95 (Scale bar 20µm). Transparent white lines show manually drawn outlines of the outer auditory cortex boundary. (C) shows FISH channel for Beta Actin, Poly A, Poly T as a control for Poly A, and Psd95 (antisense and sense strand as a control). Controls show an absence of signal as expected, PolyA shows a strong signal as expected, and a punctate signal can also be seen for endogenous Beta Actin and Psd95.

3.4 Puromycilation and Puro-PLA Experiments to Quantify Translation

After establishing that our endogenous mRNAs could be detected in layer I, we wanted to validate our ability to detect the translation of reporter constructs in distal dendrites using an alternative method, a puromycin proximity ligation assay (Puro-PLA)[88]. Puromycin is an inhibitor of translation that mimics tRNAs and covalently attaches to the newly synthesized peptide chain via a peptide bond[58].

First, we performed a puromycilation experiment to see whether we could successfully perform puromycin labelling. This was done with enhanced yellow fluorescent protein (EYFP) transduced cultured neurons. Since EYFP is a fluorescent protein derivative of GFP, as is Venus, the rationale behind using it for optimization experiments was that it could function as a proxy for our myrVenus constructs. As a negative control, we pre-incubated the neurons with anisomycin, a protein synthesis inhibitor that immobilizes translating ribosomes on the mRNA chain, effectively blocking all protein synthesis. Moreover, we also evaluated the protocol without puromycin to see whether there was any background from the antibody. We concluded that our anisomycin and no puromycin controls worked robustly, as indicated by the absence of a fluorescent signal (Fig. 15).

After these successful controls were performed, we proceeded with a PLA against puromycin and EYFP (Fig. 16). A PLA is a technique used to identify and quantify protein-protein interactions by detecting the proximity of two antibodies. The DNA ligase can bond oligos only when they are close to each other; thus, only these nearby interactions can be joined, leading to a rolling cycle amplification procedure. This process involves incorporating fluorescent molecules, which enable the visualization of the close antibody coincidence[88]. Our puro-PLA experiment was successful, as seen by the lack of signal in our negative controls and a clear punctate signal in our puromycin condition, which confirms the detection and localisation of nascent EYFP. Although Puro-PLA worked, we noticed fewer signal than expected, indicating that further optimization would be necessary before this method could be used reliably for our reporter constructs.

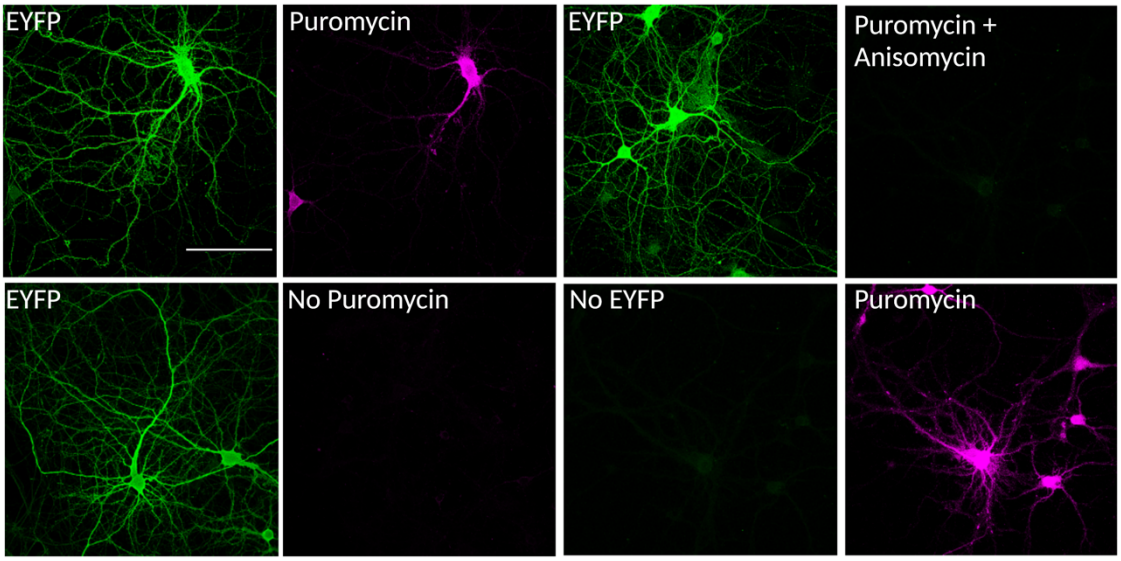

Fig. 15. Confocal images (40x oil) in cultured EYFP neurons showing effective puromycilation experiment performed by Dr. Paul Donlin-Asp (scale bar 50µm). Puromycin levels are reflective of total protein synthesis. From left to right, top to bottom: puromycin, no puromycin, puromycin with previous anisomycin treatment (protein synthesis inhibitor), no EYFP. Anisomycin and no puromycin controls worked robustly, as indicated by the absence of fluorescent signal.

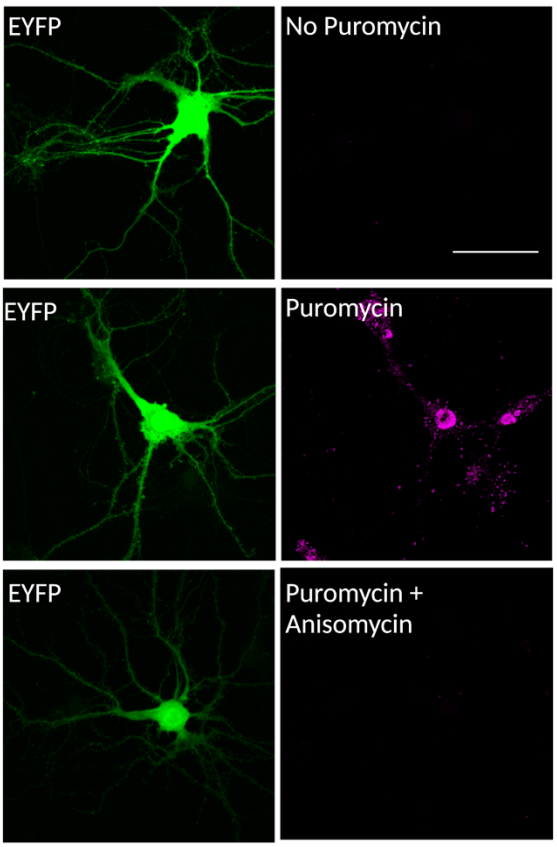

Fig. 16. Confocal images (40x in oil) in cultured EYFP neurons showing successful puromycin proximity ligation assay (puro-PLA) to visualize nascent EYFP via complementary detection with puromycin (Scale bar 50µm). Puro-PLA performed by Dr. Paul Donlin-Asp. From bottom to top: no puromycin, puromycin, puromycin with previous anisomycin treatment (protein inhibitor). Figures show that anisomycin and no puromycin controls worked robustly, and punctate signal in the puromycin condition (magenta) shows clear detection and localisation of nascent EYFP.

4. Discussion

In this research thesis, previously developed 3' UTR constructs were implemented to study whether *Beta Actin* and *Psd95* 3'UTRs drive the localisation of myrVenus mRNA into dendrites in cortical neurons in culture (Fig. 6), and in tissue (Fig. 14). In addition, the distribution of mRNAs across dendrites was analysed between UTR constructs and their endogenous mRNA equivalents (Fig. 11).

4.1 UTR Constructs and Endogenous mRNA in Cultured Neurons

The results of our FISH experiments in culture (Fig. 4-7) demonstrate that the UTR constructs tend to concentrate in dendrites more than their no UTR counterparts, confirming that these constructs serve as effective imitations of endogenous mRNA transcripts and enable the analysis of translation in remote areas. From these results, an interesting observation is the amount of no UTR mRNA we detect localising into the dendrites (Fig. 5-7), raising the question of how this localisation occurs. As this construct lacks any regulatory information controlling when and where it should be translated, it was not expected to accumulate appreciably in distal regions in the neuron. Without a UTR, the mRNA lacks the necessary signals for transportation to distal regions and will likely remain in the soma where it was transcribed. It is worth noting that the constructs are introduced into cells through viral transduction. This method of expression results in a high number of copies of the virus entering the cell, leading to an overproduction of mRNA compared to endogenous gene expression levels. This surplus of mRNA may cause a spill-over effect in the dendrites. In addition, the viral overexpression of the no UTR construct could potentially lead to the co-opting of mRNA transport mechanisms, such as coupling to endosomes and other transported cargo[89–91].

However, when observing the fractional distribution between dendritic and somatic compartments, most mRNAs were found in the soma, although considerably less for the Beta Actin and Psd95 UTR constructs (Fig. 7) This observation was expected as transcription occurs in the nucleus before mRNAs are shuttled into dendrites. Interestingly, when comparing the raw total mRNA count between constructs (Fig. 7A), the no UTR shows an overall lower puncta count. If we were to only consider the 3' UTR's role in mRNA localisation to dendrites, we would anticipate that the overall raw count of mRNAs would remain constant, resulting in nearly identical expression levels among the different

constructs. However, it is widely accepted that UTR sequences often influence mRNA stability[92,93]. More stable mRNAs result in a longer half-life for the constructs, leading to a higher number of molecules present at any given time. Therefore, a reduced mRNA half-life could explain the significantly lower total raw count of the no UTR constructs. This is consistent with previous data showing that when mRNA half-life is reduced, there is a subsequent drop in total mRNA levels[11,94–96].

We also found that the variability within the data for the reporter-infected cells was significant (Fig. 7). This variability can be attributed to various factors. The main difference is most likely the virus expression in the cells themselves. It is well appreciated that virus infection can be extremely heterogeneous within a cell population. The efficacy of expression depends on many factors that the endogenous mRNA is not subject to. For instance, the fact that constructs have no 5'UTR, no introns, and therefore no normal regulation[11]. Also, the normal regulators limiting *Beta Actin* and *Psd95* mRNA levels are lacking in the reporter constructs leading to higher and more varied expression.

In the experiments with endogenous transcripts, *Psd95* and *Beta Actin* showed a lower dendritic distribution than our *CamKII* and *PolyA* positive controls (Fig. 8-9). *PolyA* is a sequence at the 3' end of all mRNA molecules and acts as a marker for mRNA stability and transport. Therefore, it was expected that *PolyA* would have a higher puncta count because it is present in all mRNAs, including our candidate mRNAs[45]. Additionally, we expected a strong signal for *CamKII* mRNA, as this mRNA is known to be highly expressed and efficiently transported to dendrites[97]. Post-hoc Tukey tests further showed that *Psd95* had similar raw puncta counts to *Beta Actin* ($p = 0.9384$), whereas both endogenous mRNAs showed a statistically significant difference with *CamKII* ($p < 0.0001$) and *PolyA* ($p < 0.0001$), as outlined in the supplemental figures (S1). We concluded that no notable difference was observed in fractional mRNA count for our endogenous *Beta Actin* and *Psd95* in cultured cortical neurons.

Lastly, when comparing our reporter constructs to endogenous mRNA, we observed lower raw counts for the endogenous mRNAs (Fig. 10A) than our UTR constructs. As mentioned previously, this is likely attributed to the fact that we overexpressed the reporter constructs, leading to a higher quantity of mRNA in the dendrites compared to their endogenous counterparts. In fact, the fractional distributions were similar (Fig. 10B), as shown by a two-

tailed unpaired T-test analysis for *Beta Actin* (p-value 0.0893). Although *Psd95* (p-value <0.001) showed statistical significance, it should be noted that this was also a factor of having a relatively low-powered data set. In sum, we determined that our UTR reporter constructs showed higher distribution in dendrites compared to endogenous mRNA but that this was influenced by variability in our reporter data and viral overexpression. With these conclusions in mind, it is important to acknowledge that there were some limitations in the methodologies used in the analysis.

Starting from the beginning of our analysis pipeline, we used max intensity projection to quantify mRNA puncta (Methods 2.7) due to the thinness of dendrites in low-density areas. While this method effectively captures the dendritic distribution of mRNA, it may not provide an accurate representation of mRNA puncta density in regions of higher cell density due to overlapping dendrites. For instance, resolving somatic mRNA puncta was challenging due to a large amount of signal being condensed into a small space in the ROI. Alternative strategies – such as binary thresholding and intensity measurement techniques – were considered to quantify somatic mRNA, but these methods did not accurately resolve individual mRNA copies in the soma.

A more appropriate method would be to normalize the fluorescence intensity of each spot and use this measurement to estimate the total number of mRNA copies. This involves adjusting the fluorescence intensity measurement to make it comparable across different samples or conditions. This results in a more accurate assessment of mRNA copy numbers for the total fluorescence detected. However, as single-molecule FISH was not used, this approach would not have been more accurate than the one employed. An alternative option would be to create 3D renderings with Imaris software – which would be an amenable future approach.

In addition, we used a fractional distribution analysis (Methods 2.8) to account for raw puncta count variability. This method allowed us to normalize for differences, especially between our reporter constructs and endogenous mRNAs. A limitation was that our analysis was based on a limited neuronal volume subset, meaning we were under-sampling the total dendritic fraction. However, since we selected the same number of ROIs of a defined length for each group, it should not have affected the comparative outcome.

4.2 mRNA Distribution Across Dendrite Lengths

We then looked at the distribution of mRNAs across dendrite length (Fig. 11). We chose a linear regression to model the average mRNA distribution, as it was simple and allowed easy comparison between constructs.

From our results, we noticed that most puncta were found in the first 30μm of dendrite and that this constantly decreased with increasing distance from the soma, which has been seen before in other studies[14,98,99]. This pattern was consistent between our reporter *Beta Actin* UTR and *Psd95* UTR and the no UTR (Fig. 11C-D). This decreasing trend also agrees with research by Fonkeu et al. (2019)[85], who proposed a computational model for the spatial distribution of mRNAs and applied it to the endogenous protein *CaMKIIα*.

Interestingly, we noticed that while the total amount of puncta for the no UTR in the dendrites was lower, those molecules that did localise in dendrites displayed a similar distribution pattern as the *Psd95* and *Beta Actin* UTR (Fig. 11). This implies that the overexpression of the no UTR reporter probably hijacks RNA trafficking mechanisms for localisation, and most likely, the mRNAs that make it out into dendrites follow a generic distribution pattern. The observation of lower amounts of the no UTR mRNA reaching out into distal dendrites was in line with our expectations: in fact, after 20μm of dendrite, there were less than 5 average mRNA puncta per subsequent bin for the no UTR construct (Fig. 11C), which is significantly lower than our UTR reporter constructs. In addition, our reporter constructs were distributed similarly to their endogenous counterparts (Fig. 11A-B), as further reflected by the similar linear regressions (Fig. 13), showing an almost equal slope coefficient for all constructs.

From this and the other results presented, we would conclude that the UTR's function is to stabilize and localise the mRNA and that decoupling these effects is likely non-trivial. However, it is important to consider that all the constructs transduced into cells were overexpressed, making it harder to discern whether sequences within the 3' UTR alone drive mRNA localisation or if, under endogenous conditions, the stability of mRNA that the 3'UTR confers can give it time to associate with trafficking machinery to be distally localised within the neuron. This possibility is consistent with the similar distribution patterns seen for the no UTR vs UTR containing reporters, suggesting that there are no transcript-specific

distribution trajectories for mRNAs, rather that these distribute generically. Although this observation is based on a few candidate mRNAs, it is consistent with the notion that a continuous pool of mRNAs is trafficked to dendrites and that synapses capture necessary molecules during specific synaptic plasticity[47,79,100].

4.3 UTR Constructs and Endogenous mRNA in Tissue

We next focused on seeing whether our mRNA constructs were also localising in tissue slices, as they were in culture. Given the more complex nature of working *ex vivo*, we encountered some difficulties with the FISH protocol. We modified the procedures and obtained a signal for our no UTR and UTR constructs (Fig. 13). Our FISH experiments showed background noise in the tissue, with reporter mRNA signal beyond the boundaries of myrVenus protein and dendrites in the injected hemisphere (Fig. 13A). This was not seen in cells without myrVenus protein on the non-injected side (Fig. 13B). Thus, we concluded that the FISH results were not representative of mRNA distribution, as the probes were binding to the smaller-size AAV genome during hybridization leading to the detection of both mRNA and DNA in the puncta. Another concern was that the myrVenus/EYFP sequence might have the capacity to amplify the signal without the hybridization probe being present. A control experiment (data not shown) was conducted by Belquis Nassim on the myrVenus constructs without adding the probe, showing that this was the case.

Given the challenges faced in the FISH experiment against AAV-derived mRNA, our data in Fig.13 could not be used for quantification as we were not confident it only represented mRNA. Given this, a simpler question was posed: whether the endogenous mRNAs for *Beta Actin* and *Psd95* were localising in layer 1 *in vivo*. The results (Fig. 14A-B) indicate that both constructs were localising in this layer, and no major issues were encountered. In addition, our negative control experiments with *PolyT*, and *Psd95* (sense strand) worked robustly as we did not see a signal (Fig. 14C), whereas in our positive *PolyA* control showed an abundance of signal.

4.4 Puromycilation Experiments

Next, we investigated whether certain mRNAs were being translated in dendrites using a proximity ligation assay (PLA), which allowed us to detect newly synthesized proteins. We used a technique called puromycilation to add puromycin (puro) to the newly forming polypeptide chain and determined that our controls worked robustly (Fig. 15). The puro-PLA experiment was also successful, as evidenced by the absence of signal in our negative controls and a clear punctate signal in our puromycin condition (Fig. 16). Compared to a previously published experiment using puro-PLA by tom Dieck et al.[15], we did note a lower total count of puncta in our experimental setup than expected. The expression of EYFP protein is thought to have a high rate of translation[101], and we assumed this would result in higher production of the protein and a greater number of puncta detected. We also saw EYFP expressed rapidly and highly after a few days of transduction, suggesting that it was being translated robustly. However, a key difference with our experimental set-up is that we attempted to identify a fluorescent protein, not an endogenous protein, which most likely explains our lower raw counts.

5. Outlook

Overall, the work outlined herein demonstrates that the localisation and distribution of our candidate mRNA reporters are similar to their endogenous counterparts in culture. Despite being overexpressed, the reporters can localise to dendrites, indicating that the localisation of an mRNA with an untranslated region (UTR) may differ from that of an mRNA without a UTR, which could account for any observed changes in protein translation. However, we have yet to determine if this also holds *in vivo*, as the FISH technique was ineffective when analysing the reporter's infected tissue sections.

In addition, these fluorescent reporters can be used to probe the regulatory sequences necessary for their localisation. For example, new constructs can be created with modified 5'UTR or 3'UTR regions to increase or decrease mRNA stability. It would also be interesting to compare the cellular distribution of these fluorescent reporters during the induction of synaptic plasticity, such as BDNF-induced potentiation, to those with intact regulatory sequences and to their endogenous counterparts.

Moreover, we noticed that an exponential model would also be suitable for our data showing the total raw mRNA distribution along dendrite length (supplemental figures Fig. S2). Due to the high variability in each data bin, further data would be required to improve the fit. Alternatively, we could normalize the puncta count based on the predicted dendrite diameter, similar to the method described by Fonkeu et al.[85], and then apply a linear model.

Finally, following our puro-PLA experiments with EYFP, a puro-PLA assay should be performed on neurons transfected with our reporters and the no UTR control, as well as with our endogenous mRNA candidates. This assay will allow us to label and visualize the newly synthesized proteins and determine if these mRNAs are being locally translated.

In conclusion, the UTR fluorescent reporter constructs we have assessed are robust and reliable tools *in vitro*, and they exhibit great potential for evaluating local protein synthesis in a living organism. While there are still challenges to be addressed, this research has brought us closer to achieving a credible visualization of this process and has laid the foundation for future studies in this field.

6. Works Cited

(1) Holt, C. E.; Schuman, E. M. The Central Dogma Decentralized: New Perspectives on RNA Function and Local Translation in Neurons. *Neuron* **2013**, *80* (3), 648–657. https://doi.org/10.1016/j.neuron.2013.10.036.

(2) Biever, A.; Donlin-Asp, P. G.; Schuman, E. M. Local Translation in Neuronal Processes. *Curr Opin Neurobiol* **2019**, *57*, 141–148. https://doi.org/10.1016/j.conb.2019.02.008.

(3) Holt, C. E.; Martin, K. C.; Schuman, E. M. Local Translation in Neurons: Visualization and Function. *Nat Struct Mol Biol* **2019**, *26* (7), 557–566. https://doi.org/10.1038/s41594-019-0263-5.

(4) Kang, H.; Schuman, E. M. Long-Lasting Neurotrophin-Induced Enhancement of Synaptic Transmission in the Adult Hippocampus. *Science* **1995**, *267* (5204), 1658–1662. https://doi.org/10.1126/science.7886457.

(5) Maday, S.; Twelvetrees, A. E.; Moughamian, A. J.; Holzbaur, E. L. F. Axonal Transport: Cargo-Specific Mechanisms of Motility and Regulation. *Neuron* **2014**, *84* (2), 292–309. https://doi.org/10.1016/j.neuron.2014.10.019.

(6) Chaudhuri, T. K.; Paul, S. Protein-Misfolding Diseases and Chaperone-Based Therapeutic Approaches. *FEBS J* **2006**, *273* (7), 1331–1349. https://doi.org/10.1111/j.1742-4658.2006.05181.x.

(7) Bagni, C.; Zukin, R. S. A Synaptic Perspective of Fragile X Syndrome and Autism Spectrum Disorders. *Neuron* **2019**, *101* (6), 1070–1088. https://doi.org/10.1016/j.neuron.2019.02.041.

(8) Eom, T.; Antar, L. N.; Singer, R. H.; Bassell, G. J. Localization of a β-Actin Messenger Ribonucleoprotein Complex with Zipcode-Binding Protein Modulates the Density of Dendritic Filopodia and Filopodial Synapses. *Journal of Neuroscience* **2003**, *23* (32), 10433–10444.

(9) Andreassi, C.; Zimmermann, C.; Mitter, R.; Fusco, S.; De Vita, S.; Saiardi, A.; Riccio, A. An NGF-Responsive Element Targets Myo-Inositol Monophosphatase-1 MRNA to Sympathetic Neuron Axons. *Nature neuroscience* **2010**, *13* (3), 291–301.

(10) Taliaferro, J. M.; Vidaki, M.; Oliveira, R.; Olson, S.; Zhan, L.; Saxena, T.; Wang, E. T.; Graveley, B. R.; Gertler, F. B.; Swanson, M. S.; Burge, C. B. Distal Alternative Last Exons Localize MRNAs to Neural Projections. *Mol Cell* **2016**, *61* (6), 821–833. https://doi.org/10.1016/j.molcel.2016.01.020.

(11) Tushev, G.; Glock, C.; Heumüller, M.; Biever, A.; Jovanovic, M.; Schuman, E. M. Alternative 3' UTRs Modify the Localization, Regulatory Potential, Stability, and Plasticity of MRNAs in Neuronal Compartments. *Neuron* **2018**, *98* (3), 495-511.e6. https://doi.org/10.1016/j.neuron.2018.03.030.

(12) Fontes, M. M.; Guvenek, A.; Kawaguchi, R.; Zheng, D.; Huang, A.; Ho, V. M.; Chen, P. B.; Liu, X.; O'Dell, T. J.; Coppola, G. Activity-Dependent Regulation of Alternative Cleavage and Polyadenylation during Hippocampal Long-Term Potentiation. *Scientific reports* **2017**, *7* (1), 1–13.

(13) Aakalu, G.; Smith, W. B.; Nguyen, N.; Jiang, C.; Schuman, E. M. Dynamic Visualization of Local Protein Synthesis in Hippocampal Neurons. *Neuron* **2001**, *30* (2), 489–502. https://doi.org/10.1016/S0896-6273(01)00295-1.

(14) Donlin-Asp, P. G.; Polisseni, C.; Klimek, R.; Heckel, A.; Schuman, E. M. Differential Regulation of Local MRNA Dynamics and Translation Following Long-Term Potentiation and Depression. *Proceedings of the National Academy of Sciences* **2021**, *118* (13), e2017578118. https://doi.org/10.1073/pnas.2017578118.

(15) tom Dieck, S.; Kochen, L.; Hanus, C.; Heumüller, M.; Bartnik, I.; Nassim-Assir, B.; Merk, K.; Mosler, T.; Garg, S.; Bunse, S.; Phd, D.; Schuman, E. Direct Visualization of Newly Synthesized Target Proteins in Situ. *Nature methods* **2015**, *12*. https://doi.org/10.1038/nmeth.3319.

(16) Azevedo, F. A. C.; Carvalho, L. R. B.; Grinberg, L. T.; Farfel, J. M.; Ferretti, R. E. L.; Leite, R. E. P.; Jacob Filho, W.; Lent, R.; Herculano-Houzel, S. Equal Numbers of Neuronal and Nonneuronal Cells Make the Human Brain an Isometrically Scaled-up Primate Brain. *J Comp Neurol* **2009**, *513* (5), 532–541. https://doi.org/10.1002/cne.21974.

(17) Tovée, M. J. Neuronal Processing. How Fast Is the Speed of Thought? *Curr Biol* **1994**, *4* (12), 1125–1127. https://doi.org/10.1016/s0960-9822(00)00253-0.

(18) Citri, A.; Malenka, R. C. Synaptic Plasticity: Multiple Forms, Functions, and Mechanisms. *Neuropsychopharmacol* **2008**, *33* (1), 18–41. https://doi.org/10.1038/sj.npp.1301559.

(19) Lugaro, E. *I problemi odierni della psichiatria / Ernesto Lugaro*; L'indagine moderna 0003; Sandron, R. Sandron: Milano, Palermo, Napoli, Milano [etc., Milano, 1906.

(20) Pielot, R.; Smalla, K.-H.; Müller, A.; Landgraf, P.; Lehmann, A.-C.; Eisenschmidt, E.; Haus, U.-U.; Weismantel, R.; Gundelfinger, E. D.; Dieterich, D. C. SynProt: A Database for Proteins of Detergent-Resistant Synaptic Protein Preparations. *Front Synaptic Neurosci* **2012**, *4*, 1. https://doi.org/10.3389/fnsyn.2012.00001.

(21) Helm, M. S.; Dankovich, T. M.; Mandad, S.; Rammner, B.; Jähne, S.; Salimi, V.; Koerbs, C.; Leibrandt, R.; Urlaub, H.; Schikorski, T.; Rizzoli, S. O. A Large-Scale Nanoscopy and Biochemistry Analysis of Postsynaptic Dendritic Spines. *Nat Neurosci* **2021**, *24* (8), 1151–1162. https://doi.org/10.1038/s41593-021-00874-w.

(22) Good, M. C.; Zalatan, J. G.; Lim, W. A. Scaffold Proteins: Hubs for Controlling the Flow of Cellular Information. *Science* **2011**, *332* (6030), 680–686. https://doi.org/10.1126/science.1198701.

(23) Sheng, M.; Hoogenraad, C. C. The Postsynaptic Architecture of Excitatory Synapses: A More Quantitative View. *Annu. Rev. Biochem.* **2007**, *76*, 823–847.

(24) Price, J. C.; Guan, S.; Burlingame, A.; Prusiner, S. B.; Ghaemmaghami, S. Analysis of Proteome Dynamics in the Mouse Brain. *Proceedings of the National Academy of Sciences* **2010**, *107* (32), 14508–14513.

(25) Cohen, L. D.; Zuchman, R.; Sorokina, O.; Müller, A.; Dieterich, D. C.; Armstrong, J. D.; Ziv, T.; Ziv, N. E. Metabolic Turnover of Synaptic Proteins: Kinetics, Interdependencies and Implications for Synaptic Maintenance. *PloS one* **2013**, *8* (5), e63191.

(26) Flexner, L. B.; Flexner, J. B. Effect of Acetoxycycloheximide and of an Acetoxycycloheximide-Puromycin Mixture on Cerebral Protein Synthesis and Memory in Mice. *Proceedings of the National Academy of Sciences of the United States of America* **1966**, *55* (2), 369–374.

(27) Alberini, C. M.; Ghirardl, M.; Metz, R.; Kandel, E. R. C/EBP Is an Immediate-Early Gene Required for the Consolidation of Long-Term Facilitation in Aplysia. *Cell* **1994**, *76* (6), 1099–1114. https://doi.org/10.1016/0092-8674(94)90386-7.

(28) Costa-Mattioli, M.; Gobert, D.; Harding, H.; Herdy, B.; Azzi, M.; Bruno, M.; Bidinosti, M.; Mamou, C. B.; Marcinkiewicz, E.; Yoshida, M.; Imataka, H.; Claudio Cuello, A.; Seidah, N.; Sossin, W.; Lacaille, J.-C.; Ron, D.; Nader, K.; Sonenberg, N. Translational Control of Hippocampal Synaptic Plasticity and Memory by the EIF2α Kinase, GCN2. *Nature* **2005**, *436* (7054), 1166–1173. https://doi.org/10.1038/nature03897.

(29) Banko, J. L.; Hou, L.; Poulin, F.; Sonenberg, N.; Klann, E. Regulation of Eukaryotic Initiation Factor 4E by Converging Signaling Pathways during Metabotropic

Glutamate Receptor-Dependent Long-Term Depression. *J Neurosci* **2006**, *26* (8), 2167–2173. https://doi.org/10.1523/JNEUROSCI.5196-05.2006.

(30) Berger-Sweeney, J.; Zearfoss, N. R.; Richter, J. D. Reduced Extinction of Hippocampal-Dependent Memories in CPEB Knockout Mice. *Learn Mem* **2006**, *13* (1), 4–7. https://doi.org/10.1101/lm.73706.

(31) Bartlett, W. P.; Banker, G. A. An Electron Microscopic Study of the Development of Axons and Dendrites by Hippocampal Neurons in Culture. I. Cells Which Develop without Intercellular Contacts. *Journal of Neuroscience* **1984**, *4* (8), 1944–1953.

(32) Grafstein, B.; Forman, D. S. Intracellular Transport in Neurons. *Physiological reviews* **1980**, *60* (4), 1167–1283.

(33) Hafner, A.-S.; Donlin-Asp, P. G.; Leitch, B.; Herzog, E.; Schuman, E. M. Local Protein Synthesis Is a Ubiquitous Feature of Neuronal Pre- and Postsynaptic Compartments. *Science* **2019**, *364* (6441), eaau3644. https://doi.org/10.1126/science.aau3644.

(34) Koenig, E. Synthetic Mechanisms in the Axon. 3. Stimulation of Acetylcholinesterase Synthesis by Actinomycin-D in the Hypoglossal Nerve. *J Neurochem* **1967**, *14* (4), 429–435. https://doi.org/10.1111/j.1471-4159.1967.tb09541.x.

(35) Morgan, I. G.; Austin, L. Synaptosomal Protein Synthesis in a Cell-Free System*. *Journal of Neurochemistry* **1968**, *15* (1), 41–51. https://doi.org/10.1111/j.1471-4159.1968.tb06172.x.

(36) Steward, O.; Levy, W. B. Preferential Localization of Polyribosomes under the Base of Dendritic Spines in Granule Cells of the Dentate Gyrus. *J. Neurosci.* **1982**, *2* (3), 284–291. https://doi.org/10.1523/JNEUROSCI.02-03-00284.1982.

(37) Ostroff, L. E.; Cain, C. K.; Jindal, N.; Dar, N.; Ledoux, J. E. Stability of Presynaptic Vesicle Pools and Changes in Synapse Morphology in the Amygdala Following Fear Learning in Adult Rats. *Journal of Comparative Neurology* **2012**, *520* (2), 295–314. https://doi.org/10.1002/cne.22691.

(38) Ostroff, L. E.; Watson, D. J.; Cao, G.; Parker, P. H.; Smith, H.; Harris, K. M. Shifting Patterns of Polyribosome Accumulation at Synapses over the Course of Hippocampal Long-Term Potentiation. *Hippocampus* **2018**, *28* (6), 416–430. https://doi.org/10.1002/hipo.22841.

(39) McFarlane, S.; McNeill, L.; Holt, C. E. FGF Signaling and Target Recognition in the Developing Xenopus Visual System. *Neuron* **1995**, *15* (5), 1017–1028. https://doi.org/10.1016/0896-6273(95)90091-8.

(40) McFarlane, S.; Cornel, E.; Amaya, E.; Holt, C. E. Inhibition of FGF Receptor Activity in Retinal Ganglion Cell Axons Causes Errors in Target Recognition. *Neuron* **1996**, *17* (2), 245–254. https://doi.org/10.1016/S0896-6273(00)80156-7.

(41) Kang, H.; Schuman, E. M. A Requirement for Local Protein Synthesis in Neurotrophin-Induced Hippocampal Synaptic Plasticity. *Science* **1996**, *273* (5280), 1402–1406. https://doi.org/10.1126/science.273.5280.1402.

(42) Huber, K. M.; Kayser, M. S.; Bear, M. F. Role for Rapid Dendritic Protein Synthesis in Hippocampal MGluR-Dependent Long-Term Depression. *Science* **2000**, *288* (5469), 1254–1257. https://doi.org/10.1126/science.288.5469.1254.

(43) Glock, C.; Biever, A.; Tushev, G.; Nassim-Assir, B.; Kao, A.; Bartnik, I.; tom Dieck, S.; Schuman, E. M. The Translatome of Neuronal Cell Bodies, Dendrites, and Axons. *Proceedings of the National Academy of Sciences* **2021**, *118* (43), e2113929118. https://doi.org/10.1073/pnas.2113929118.

(44) Hafner, A.-S.; Donlin-Asp, P. G.; Leitch, B.; Herzog, E.; Schuman, E. M. Local Protein Synthesis Is a Ubiquitous Feature of Neuronal Pre- and Postsynaptic Compartments. *Science* **2019**, *364* (6441), eaau3644. https://doi.org/10.1126/science.aau3644.

(45) Tian, B.; Manley, J. L. Alternative Polyadenylation of MRNA Precursors. *Nat Rev Mol Cell Biol* **2017**, *18* (1), 18–30. https://doi.org/10.1038/nrm.2016.116.
(46) Miura, P.; Shenker, S.; Andreu-Agullo, C.; Westholm, J. O.; Lai, E. C. Widespread and Extensive Lengthening of 3′ UTRs in the Mammalian Brain. *Genome Res.* **2013**, *23* (5), 812–825. https://doi.org/10.1101/gr.146886.112.
(47) Doyle, M.; Kiebler, M. A. Mechanisms of Dendritic MRNA Transport and Its Role in Synaptic Tagging. *EMBO J* **2011**, *30* (17), 3540–3552. https://doi.org/10.1038/emboj.2011.278.
(48) Yoon, Y. J.; Wu, B.; Buxbaum, A. R.; Das, S.; Tsai, A.; English, B. P.; Grimm, J. B.; Lavis, L. D.; Singer, R. H. Glutamate-Induced RNA Localization and Translation in Neurons. *Proc Natl Acad Sci U S A* **2016**, *113* (44), E6877–E6886. https://doi.org/10.1073/pnas.1614267113.
(49) Kirschman, J. L.; Bhosle, S.; Vanover, D.; Blanchard, E. L.; Loomis, K. H.; Zurla, C.; Murray, K.; Lam, B. C.; Santangelo, P. J. Characterizing Exogenous MRNA Delivery, Trafficking, Cytoplasmic Release and RNA–Protein Correlations at the Level of Single Cells. *Nucleic Acids Research* **2017**, *45* (12), e113. https://doi.org/10.1093/nar/gkx290.
(50) Martin, K. C.; Casadio, A.; Zhu, H.; Yaping, E.; Rose, J. C.; Chen, M.; Bailey, C. H.; Kandel, E. R. Synapse-Specific, Long-Term Facilitation of Aplysia Sensory to Motor Synapses: A Function for Local Protein Synthesis in Memory Storage. *Cell* **1997**, *91* (7), 927–938.
(51) Yoon, B. C.; Jung, H.; Dwivedy, A.; O'Hare, C. M.; Zivraj, K. H.; Holt, C. E. Local Translation of Extranuclear Lamin B Promotes Axon Maintenance. *Cell* **2012**, *148* (4), 752–764.
(52) Campbell, D. S.; Holt, C. E. Chemotropic Responses of Retinal Growth Cones Mediated by Rapid Local Protein Synthesis and Degradation. *Neuron* **2001**, *32* (6), 1013–1026.
(53) Eng, H.; Lund, K.; Campenot, R. B. Synthesis of β-Tubulin, Actin, and Other Proteins in Axons of Sympathetic Neurons in Compartmented Cultures. *Journal of Neuroscience* **1999**, *19* (1), 1–9.
(54) Heiman, M.; Schaefer, A.; Gong, S.; Peterson, J. D.; Day, M.; Ramsey, K. E.; Suárez-Fariñas, M.; Schwarz, C.; Stephan, D. A.; Surmeier, D. J.; Greengard, P.; Heintz, N. A Translational Profiling Approach for the Molecular Characterization of CNS Cell Types. *Cell* **2008**, *135* (4), 738–748. https://doi.org/10.1016/j.cell.2008.10.028.
(55) Shigeoka, T.; Jung, H.; Jung, J.; Turner-Bridger, B.; Ohk, J.; Lin, J. Q.; Amieux, P. S.; Holt, C. E. Dynamic Axonal Translation in Developing and Mature Visual Circuits. *Cell* **2016**, *166* (1), 181–192. https://doi.org/10.1016/j.cell.2016.05.029.
(56) Dieterich, D. C.; Link, A. J.; Graumann, J.; Tirrell, D. A.; Schuman, E. M. Selective Identification of Newly Synthesized Proteins in Mammalian Cells Using Bioorthogonal Noncanonical Amino Acid Tagging (BONCAT). *Proc Natl Acad Sci U S A* **2006**, *103* (25), 9482–9487. https://doi.org/10.1073/pnas.0601637103.
(57) Dieterich, D. C.; Hodas, J. J. L.; Gouzer, G.; Shadrin, I. Y.; Ngo, J. T.; Triller, A.; Tirrell, D. A.; Schuman, E. M. In Situ Visualization and Dynamics of Newly Synthesized Proteins in Rat Hippocampal Neurons. *Nat Neurosci* **2010**, *13* (7), 897–905. https://doi.org/10.1038/nn.2580.
(58) Yarmolinsky, M. B.; Haba, G. L. D. L. Inhibition by Puromycin of Amino Acid Incorporation into Protein. *Proceedings of the National Academy of Sciences* **1959**, *45* (12), 1721–1729.
(59) Müller-Taubenberger, A. Application of Fluorescent Protein Tags as Reporters in Live-Cell Imaging Studies. *Methods Mol Biol* **2006**, *346*, 229–246. https://doi.org/10.1385/1-59745-144-4:229.

(60) Mayford, M.; Baranes, D.; Podsypanina, K.; Kandel, E. R. The 3′-Untranslated Region of CaMKIIα Is a Cis-Acting Signal for the Localization and Translation of MRNA in Dendrites. *Proceedings of the National Academy of Sciences* **1996**, *93* (23), 13250–13255.

(61) Mori, Y.; Imaizumi, K.; Katayama, T.; Yoneda, T.; Tohyama, M. Two Cis-Acting Elements in the 3′ Untranslated Region of α-CaMKII Regulate Its Dendritic Targeting. *Nat Neurosci* **2000**, *3* (11), 1079–1084. https://doi.org/10.1038/80591.

(62) Wang, D. O.; Kim, S. M.; Zhao, Y.; Hwang, H.; Miura, S. K.; Sossin, W. S.; Martin, K. C. Synapse- and Stimulus-Specific Local Translation during Long-Term Neuronal Plasticity. *Science* **2009**, *324* (5934), 1536–1540. https://doi.org/10.1126/science.1173205.

(63) Leung, K.-M.; van Horck, F. P. G.; Lin, A. C.; Allison, R.; Standart, N.; Holt, C. E. Asymmetrical Beta-Actin MRNA Translation in Growth Cones Mediates Attractive Turning to Netrin-1. *Nat Neurosci* **2006**, *9* (10), 1247–1256. https://doi.org/10.1038/nn1775.

(64) Tatavarty, V.; Ifrim, M. F.; Levin, M.; Korza, G.; Barbarese, E.; Yu, J.; Carson, J. H. Single-Molecule Imaging of Translational Output from Individual RNA Granules in Neurons. *Mol Biol Cell* **2012**, *23* (5), 918–929. https://doi.org/10.1091/mbc.E11-07-0622.

(65) Ströhl, F.; Lin, J. Q.; Laine, R. F.; Wong, H. H.-W.; Urbančič, V.; Cagnetta, R.; Holt, C. E.; Kaminski, C. F. Single Molecule Translation Imaging Visualizes the Dynamics of Local β-Actin Synthesis in Retinal Axons. *Sci Rep* **2017**, *7* (1), 709. https://doi.org/10.1038/s41598-017-00695-7.

(66) Wong, H. H.-W.; Lin, J. Q.; Ströhl, F.; Roque, C. G.; Cioni, J.-M.; Cagnetta, R.; Turner-Bridger, B.; Laine, R. F.; Harris, W. A.; Kaminski, C. F.; Holt, C. E. RNA Docking and Local Translation Regulate Site-Specific Axon Remodeling In Vivo. *Neuron* **2017**, *95* (4), 852-868.e8. https://doi.org/10.1016/j.neuron.2017.07.016.

(67) Shin, J. N.; Doron, G.; Larkum, M. E. Neocortical Layer 1 - The Memory Layer? *Science* **2021**, *374* (6567), 538–539. https://doi.org/10.1126/science.abk1859.

(68) Lifland, A. W.; Zurla, C.; Yu, J.; Santangelo, P. J. Dynamics of Native β-Actin MRNA Transport in the Cytoplasm. *Traffic* **2011**, *12* (8), 1000–1011. https://doi.org/10.1111/j.1600-0854.2011.01209.x.

(69) Mikl, M.; Vendra, G.; Kiebler, M. A. Independent Localization of MAP2, CaMKIIα and β-Actin RNAs in Low Copy Numbers. *EMBO reports* **2011**, *12* (10), 1077–1084. https://doi.org/10.1038/embor.2011.149.

(70) Ross, A. F.; Oleynikov, Y.; Kislauskis, E. H.; Taneja, K. L.; Singer, R. H. Characterization of a Beta-Actin MRNA Zipcode-Binding Protein. *Molecular and Cellular Biology* **1997**, *17* (4), 2158–2165. https://doi.org/10.1128/MCB.17.4.2158.

(71) Gu, W.; Pan, F.; Zhang, H.; Bassell, G. J.; Singer, R. H. A Predominantly Nuclear Protein Affecting Cytoplasmic Localization of β-Actin MRNA in Fibroblasts and Neurons. *The Journal of cell biology* **2002**, *156* (1), 41–52.

(72) Zhang, H. L.; Eom, T.; Oleynikov, Y.; Shenoy, S. M.; Liebelt, D. A.; Dictenberg, J. B.; Singer, R. H.; Bassell, G. J. Neurotrophin-Induced Transport of a β-Actin MRNP Complex Increases β-Actin Levels and Stimulates Growth Cone Motility. *Neuron* **2001**, *31* (2), 261–275.

(73) Keith, D.; El-Husseini, A. Excitation Control: Balancing PSD-95 Function at the Synapse. *Frontiers in Molecular Neuroscience* **2008**, *1*.

(74) Vyas, Y.; Montgomery, J. M. The Role of Postsynaptic Density Proteins in Neural Degeneration and Regeneration. *Neural Regen Res* **2016**, *11* (6), 906–907. https://doi.org/10.4103/1673-5374.184481.

(75) Krichevsky, A. M.; Kosik, K. S. Neuronal RNA Granules: A Link between RNA Localization and Stimulation-Dependent Translation. *Neuron* **2001**, *32* (4), 683–696. https://doi.org/10.1016/S0896-6273(01)00508-6.
(76) Todd, P. K.; Mack, K. J.; Malter, J. S. The Fragile X Mental Retardation Protein Is Required for Type-I Metabotropic Glutamate Receptor-Dependent Translation of PSD-95. *Proc Natl Acad Sci U S A* **2003**, *100* (24), 14374–14378. https://doi.org/10.1073/pnas.2336265100.
(77) Muddashetty, R. S.; Nalavadi, V. C.; Gross, C.; Yao, X.; Xing, L.; Laur, O.; Warren, S. T.; Bassell, G. J. Reversible Inhibition of PSD-95 MRNA Translation by MiR-125a, FMRP Phosphorylation, and MGluR Signaling. *Mol Cell* **2011**, *42* (5), 673–688. https://doi.org/10.1016/j.molcel.2011.05.006.
(78) Hafner, A.-S.; Penn, A. C.; Grillo-Bosch, D.; Retailleau, N.; Poujol, C.; Philippat, A.; Coussen, F.; Sainlos, M.; Opazo, P.; Choquet, D. Lengthening of the Stargazin Cytoplasmic Tail Increases Synaptic Transmission by Promoting Interaction to Deeper Domains of PSD-95. *Neuron* **2015**, *86* (2), 475–489. https://doi.org/10.1016/j.neuron.2015.03.013.
(79) Buxbaum, A. R.; Wu, B.; Singer, R. H. Single β-Actin MRNA Detection in Neurons Reveals a Mechanism for Regulating Its Translatability. *Science* **2014**, *343* (6169), 419–422. https://doi.org/10.1126/science.1242939.
(80) Johnson, D. R.; Bhatnagar, R. S.; Knoll, L. J.; Gordon, J. I. Genetic and Biochemical Studies of Protein N-Myristoylation. *Annual Review of Biochemistry* **1994**, *63* (1), 869–914. https://doi.org/10.1146/annurev.bi.63.070194.004253.
(81) *ViewRNA™ ISH Cell Assay Kit*. https://www.thermofisher.com/order/catalog/product/QVC0001 (accessed 2022-10-17).
(82) Otsu, N. A Threshold Selection Method from Gray-Level Histograms. *IEEE Trans. Syst., Man, Cybern.* **1979**, *9* (1), 62–66. https://doi.org/10.1109/TSMC.1979.4310076.
(83) Schneider, C. A.; Rasband, W. S.; Eliceiri, K. W. NIH Image to ImageJ: 25 Years of Image Analysis. *Nat Methods* **2012**, *9* (7), 671–675.
(84) Sánchez, C.; Díaz-Nido, J.; Avila, J. Phosphorylation of Microtubule-Associated Protein 2 (MAP2) and Its Relevance for the Regulation of the Neuronal Cytoskeleton Function. *Prog Neurobiol* **2000**, *61* (2), 133–168. https://doi.org/10.1016/s0301-0082(99)00046-5.
(85) Fonkeu, Y.; Kraynyukova, N.; Hafner, A.-S.; Kochen, L.; Sartori, F.; Schuman, E. M.; Tchumatchenko, T. How MRNA Localization and Protein Synthesis Sites Influence Dendritic Protein Distribution and Dynamics. *Neuron* **2019**, *103* (6), 1109-1122.e7. https://doi.org/10.1016/j.neuron.2019.06.022.
(86) Gusel'nikova, V. V.; Korzhevskiy, D. E. NeuN As a Neuronal Nuclear Antigen and Neuron Differentiation Marker. *Acta Naturae* **2015**, *7* (2), 42–47.
(87) Blanco-Urrejola, M.; Gaminde-Blasco, A.; Gamarra, M.; de la Cruz, A.; Vecino, E.; Alberdi, E.; Baleriola, J. RNA Localization and Local Translation in Glia in Neurological and Neurodegenerative Diseases: Lessons from Neurons. *Cells* **2021**, *10* (3), 632. https://doi.org/10.3390/cells10030632.
(88) Fredriksson, S.; Gullberg, M.; Jarvius, J.; Olsson, C.; Pietras, K.; Gústafsdóttir, S. M.; Ostman, A.; Landegren, U. Protein Detection Using Proximity-Dependent DNA Ligation Assays. *Nat Biotechnol* **2002**, *20* (5), 473–477. https://doi.org/10.1038/nbt0502-473.
(89) Palacios, I. M. How Does an MRNA Find Its Way? Intracellular Localisation of Transcripts. *Seminars in Cell & Developmental Biology* **2007**, *18* (2), 163–170. https://doi.org/10.1016/j.semcdb.2007.01.008.

(90) Kiebler, M. A.; DesGroseillers, L. Molecular Insights into MRNA Transport and Local Translation in the Mammalian Nervous System. *Neuron* **2000**, *25* (1), 19–28. https://doi.org/10.1016/S0896-6273(00)80868-5.
(91) Cioni, J.-M.; Lin, J. Q.; Holtermann, A. V.; Koppers, M.; Jakobs, M. A. H.; Azizi, A.; Turner-Bridger, B.; Shigeoka, T.; Franze, K.; Harris, W. A.; Holt, C. E. Late Endosomes Act as MRNA Translation Platforms and Sustain Mitochondria in Axons. *Cell* **2019**, *176* (1–2), 56-72.e15. https://doi.org/10.1016/j.cell.2018.11.030.
(92) Mishima, Y.; Tomari, Y. Codon Usage and 3′ UTR Length Determine Maternal MRNA Stability in Zebrafish. *Molecular Cell* **2016**, *61* (6), 874–885. https://doi.org/10.1016/j.molcel.2016.02.027.
(93) Rasekhian, M.; Roohvand, F.; Habtemariam, S.; Marzbany, M.; Kazemimanesh, M. The Role of 3'UTR of RNA Viruses on MRNA Stability and Translation Enhancement. *Mini Reviews in Medicinal Chemistry* **2021**, *21* (16), 2389–2398. https://doi.org/10.2174/1389557521666210217092305.
(94) Chan, L. Y.; Mugler, C. F.; Heinrich, S.; Vallotton, P.; Weis, K. Non-Invasive Measurement of MRNA Decay Reveals Translation Initiation as the Major Determinant of MRNA Stability. *eLife* **2018**, *7*, e32536. https://doi.org/10.7554/eLife.32536.
(95) Bernstein, J. A.; Khodursky, A. B.; Lin, P.-H.; Lin-Chao, S.; Cohen, S. N. Global Analysis of MRNA Decay and Abundance in Escherichia Coli at Single-Gene Resolution Using Two-Color Fluorescent DNA Microarrays. *Proceedings of the National Academy of Sciences* **2002**, *99* (15), 9697–9702. https://doi.org/10.1073/pnas.112318199.
(96) Narsai, R.; Howell, K. A.; Millar, A. H.; O'Toole, N.; Small, I.; Whelan, J. Genome-Wide Analysis of MRNA Decay Rates and Their Determinants in Arabidopsis Thaliana. *Plant Cell* **2007**, *19* (11), 3418–3436. https://doi.org/10.1105/tpc.107.055046.
(97) Cajigas, I. J.; Tushev, G.; Will, T. J.; tom Dieck, S.; Fuerst, N.; Schuman, E. M. The Local Transcriptome in the Synaptic Neuropil Revealed by Deep Sequencing and High-Resolution Imaging. *Neuron* **2012**, *74* (3), 453–466. https://doi.org/10.1016/j.neuron.2012.02.036.
(98) Akbalik, G.; Langebeck-Jensen, K.; Tushev, G.; Sambandan, S.; Rinne, J.; Epstein, I.; Cajigas, I.; Vlatkovic, I.; Schuman, E. M. Visualization of Newly Synthesized Neuronal RNA in Vitro and in Vivo Using Click-Chemistry. *RNA Biology* **2017**, *14* (1), 20–28. https://doi.org/10.1080/15476286.2016.1251541.
(99) Farris, S.; Lewandowski, G.; Cox, C. D.; Steward, O. Selective Localization of Arc MRNA in Dendrites Involves Activity- and Translation-Dependent MRNA Degradation. *J Neurosci* **2014**, *34* (13), 4481–4493. https://doi.org/10.1523/JNEUROSCI.4944-13.2014.
(100) Welte, M. A. Bidirectional Transport along Microtubules. *Current Biology* **2004**, *14* (13), R525–R537. https://doi.org/10.1016/j.cub.2004.06.045.
(101) *Yellow Fluorescent Protein - an overview | ScienceDirect Topics*. https://www.sciencedirect.com/topics/biochemistry-genetics-and-molecular-biology/yellow-fluorescent-protein (accessed 2023-02-04).

7. Supplemental Figures

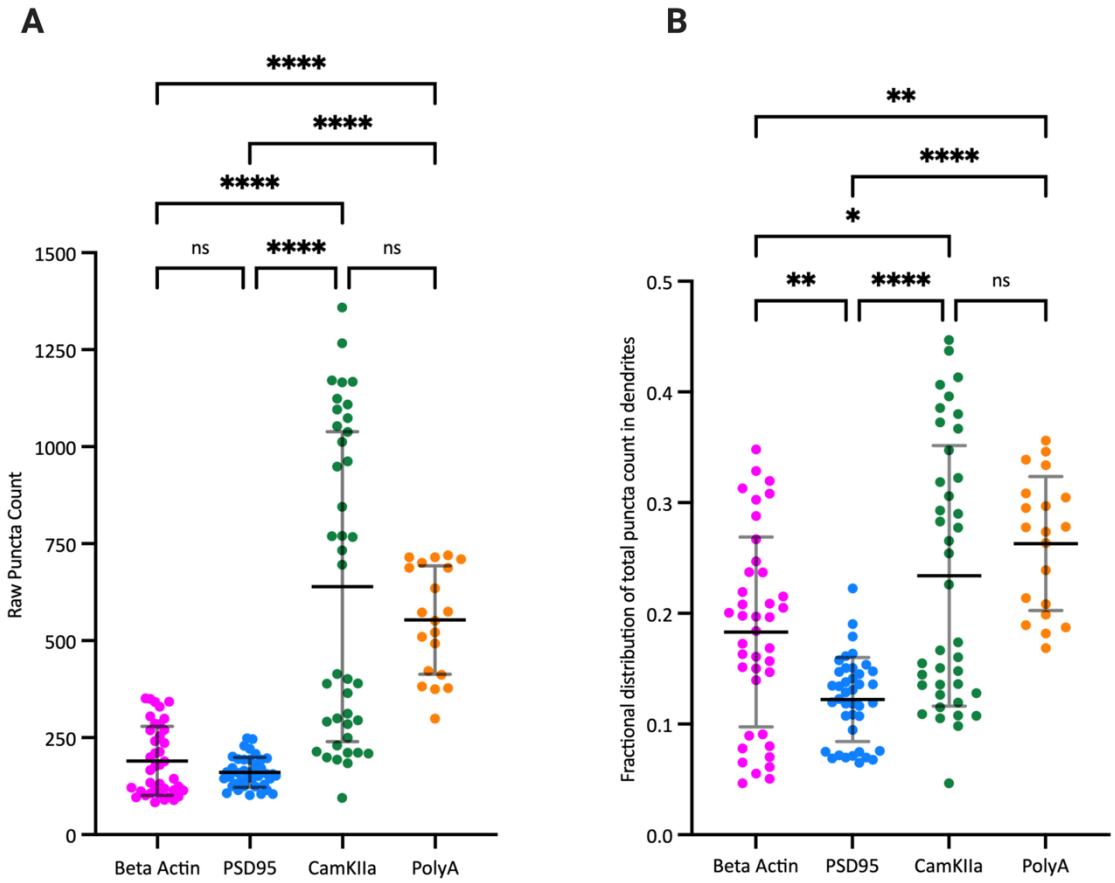

Fig. S1. Puncta distribution in dendrites for endogenous mRNA candidates Beta Actin, Psd95, CamKII and PolyA in cortical cultured cells (same data set as Fig. 9). (A) Raw counts in dendrites between show different averages between the positive controls and our candidate mRNAs, as determined by post-hoc Tukey test: Beta Actin vs CamKII (p-value <0.0001), Beta Actin vs PolyA (p-value <0.0001), Psd95 vs CamKII (p-value < 0.0001), Psd95 vs PolyA (p-value < 0.0001). However, no statistical difference was seen between candidate mRNAs and positive controls, as also determined by post-hoc Tukey test: Beta Actin vs Psd95 (p-value = 0.9384), CamKII vs PolyA (p-value = 0.5091) (B) Analysis of the fractional distribution of puncta in dendrites show a reduced statistical difference as shown by post-hoc Tukey test: : Beta Actin vs CamKII (p-value = 0.0375), Beta Actin vs PolyA (p-value = 0.0037), Psd95 vs CamKII (p-value < 0.0001), Psd95 vs PolyA (p-value < 0.0001). Beta Actin vs Psd95 (p-value = 0.0078), CamKII vs PolyA (p-value = 0.5839)

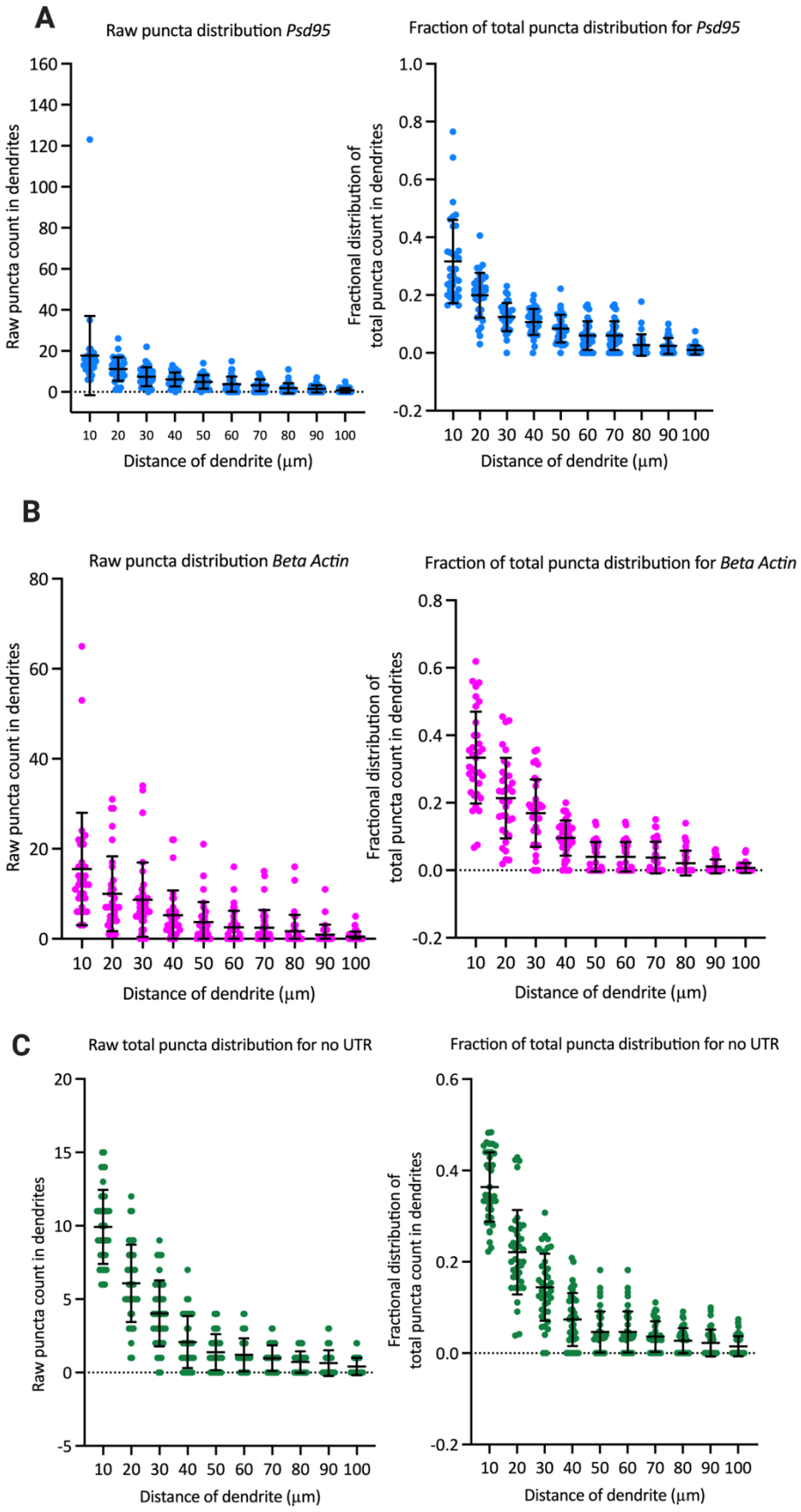

Fig. S2. Total puncta distribution in dendrites for reporter mRNA candidates Beta Actin, Psd95, and no UTR in cortical cultured cells (same data set as Fig.11). (A) Total raw counts (left) and fractional distribution (right) in dendrites for Psd95 (B) Beta Actin and (C) no UTR.